

Cosmic Ray Origin and Anisotropy measurement by the Pierre Auger Observatory

1. Recent Observations
2. Some General Considerations on Anisotropies
3. Implications and Detailed Modelling
4. Conclusions

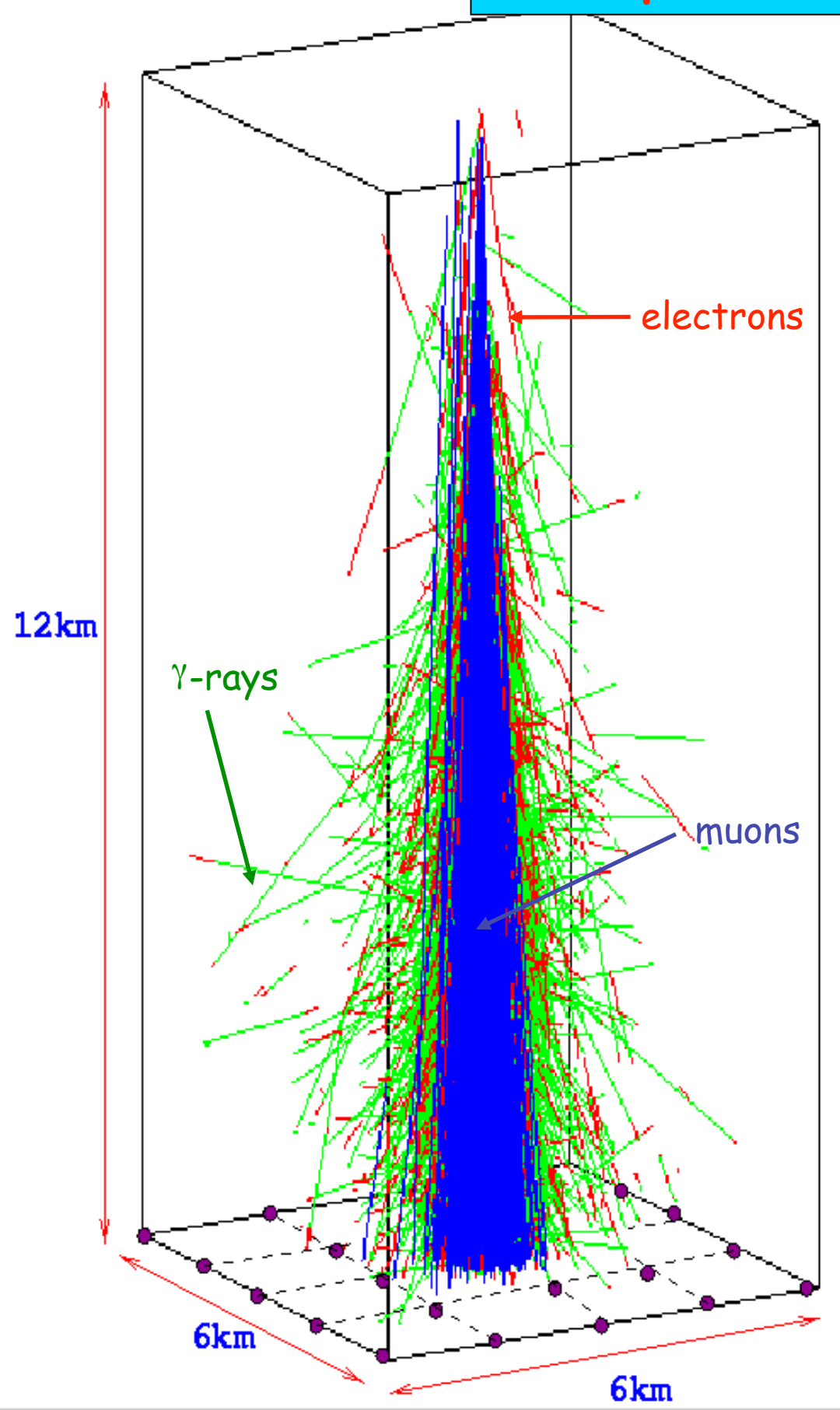


Günter Sigl

II. Institut theoretische Physik, Universität Hamburg

La Thuile 2019

Atmospheric Showers and their Detection

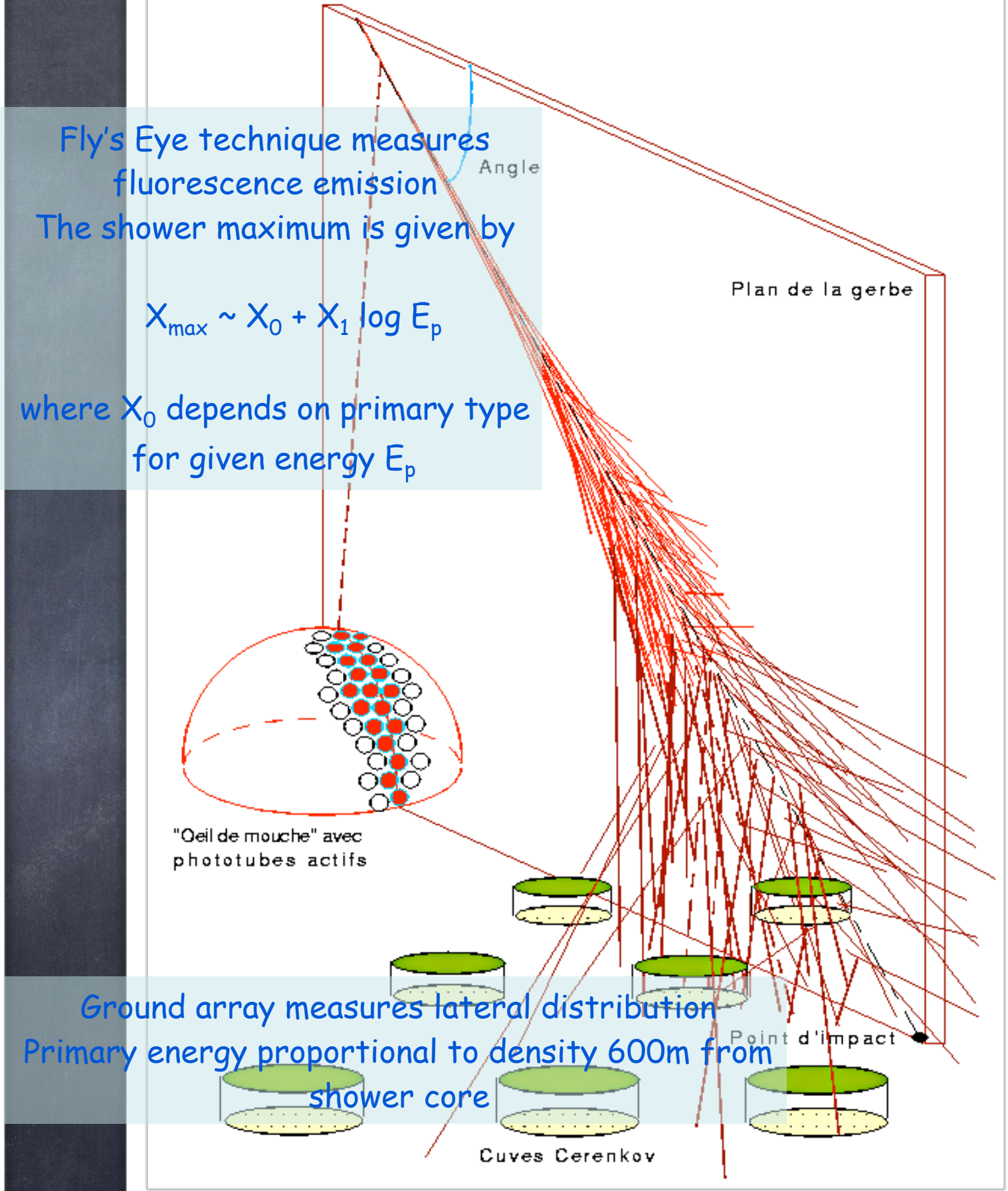


Fly's Eye technique measures fluorescence emission

The shower maximum is given by

$$X_{\max} \sim X_0 + X_1 \log E_p$$

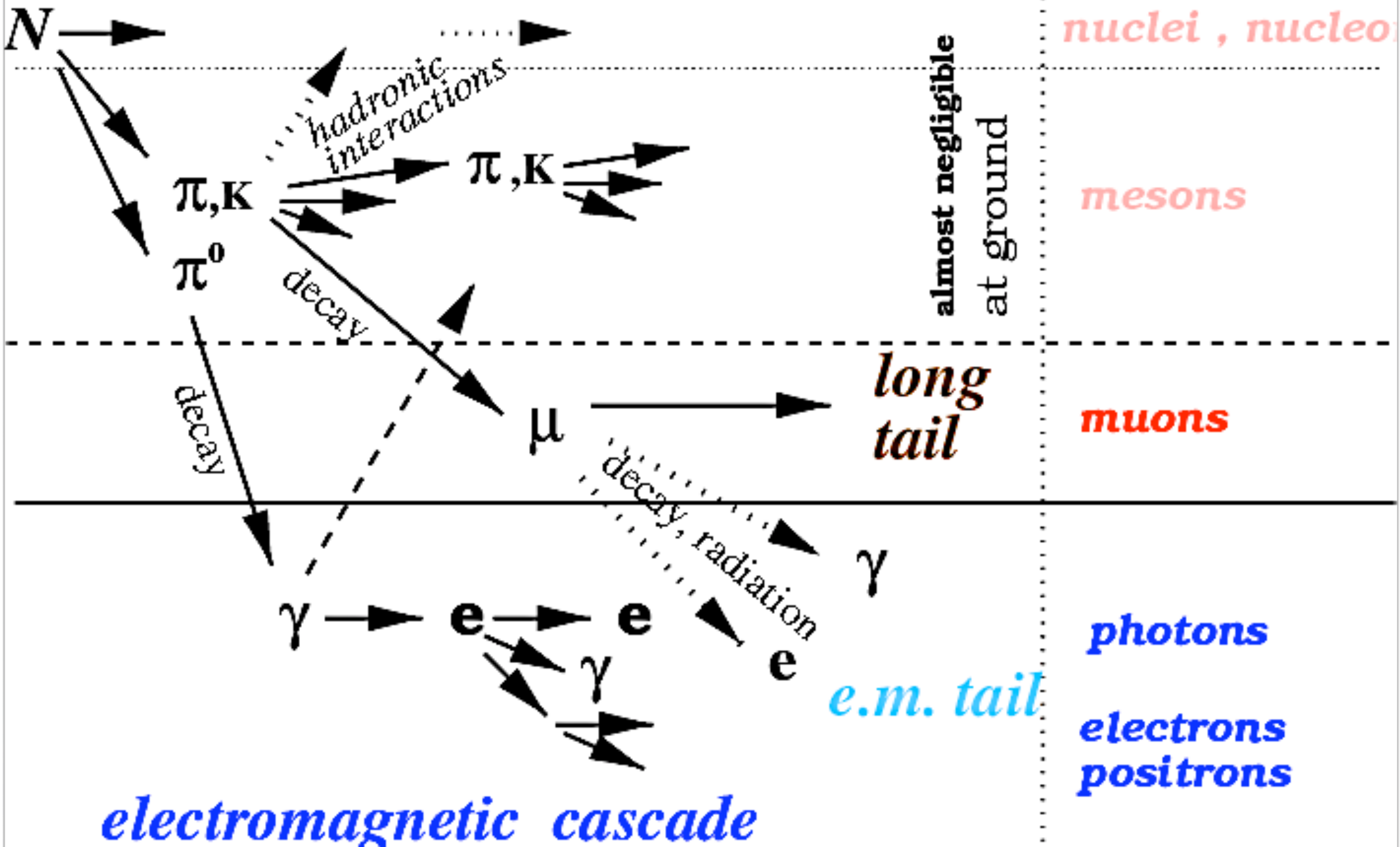
where X_0 depends on primary type for given energy E_p

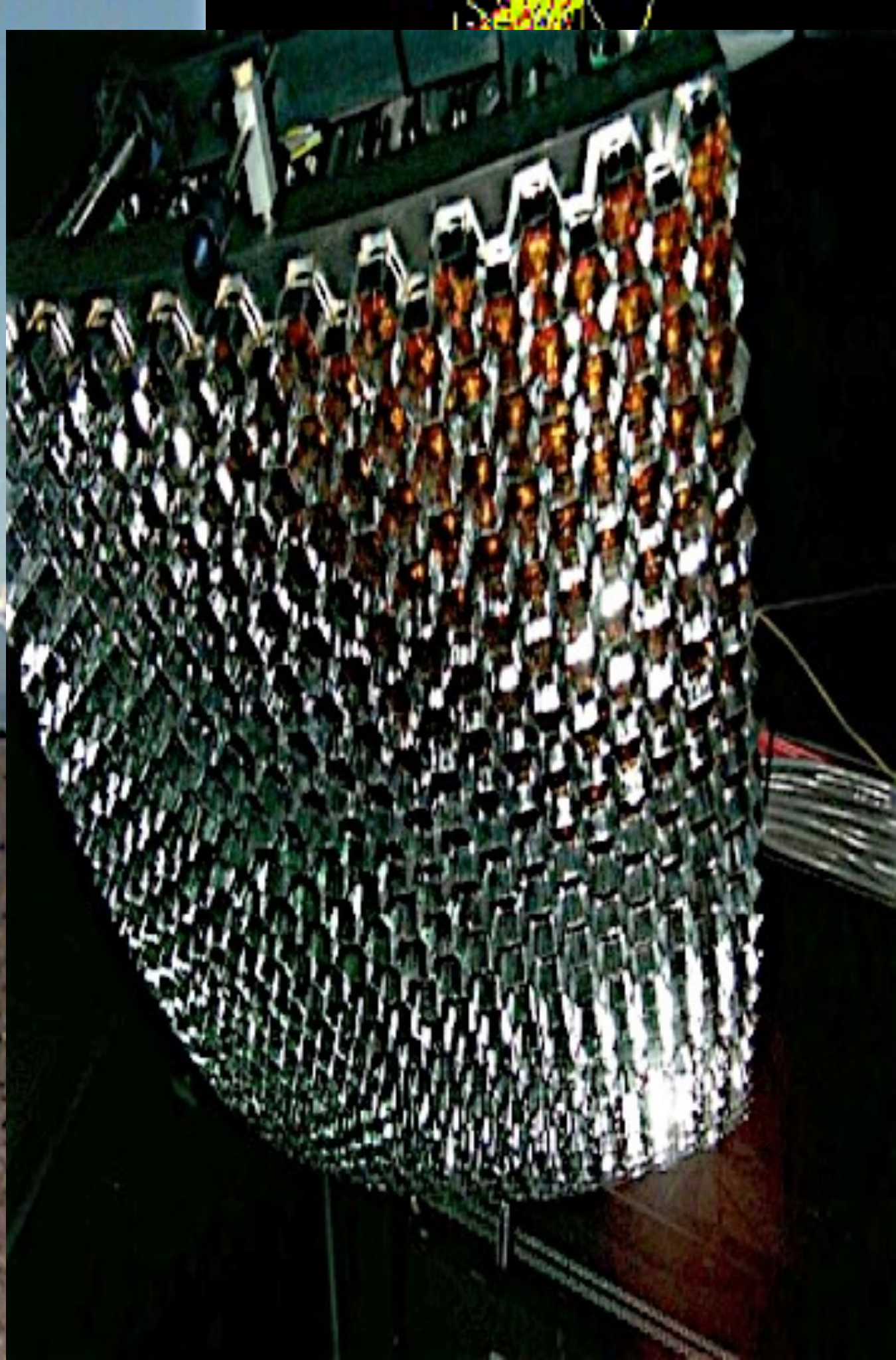


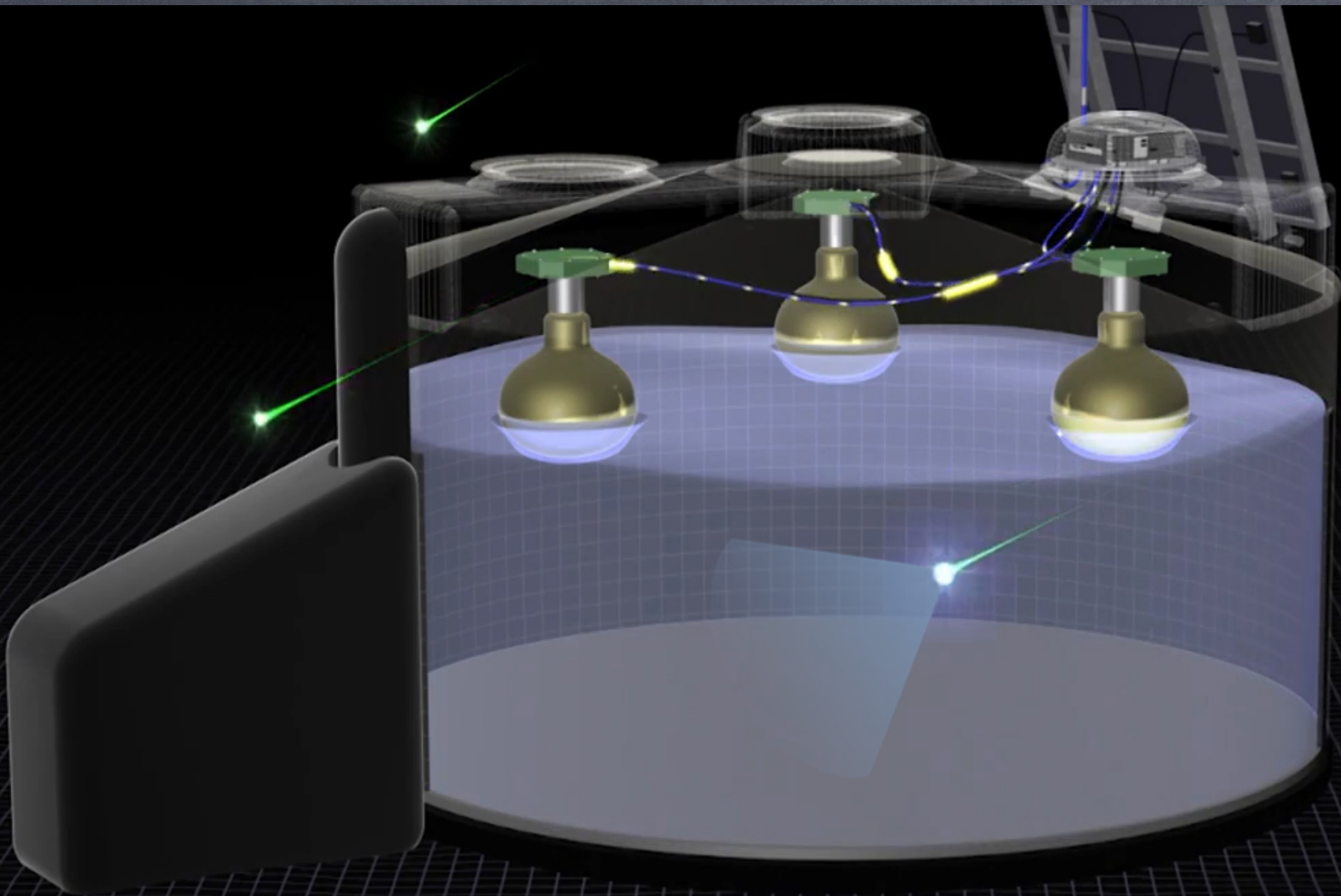
Ground array measures lateral distribution

Primary energy proportional to density 600m from shower core

hadronic cascade







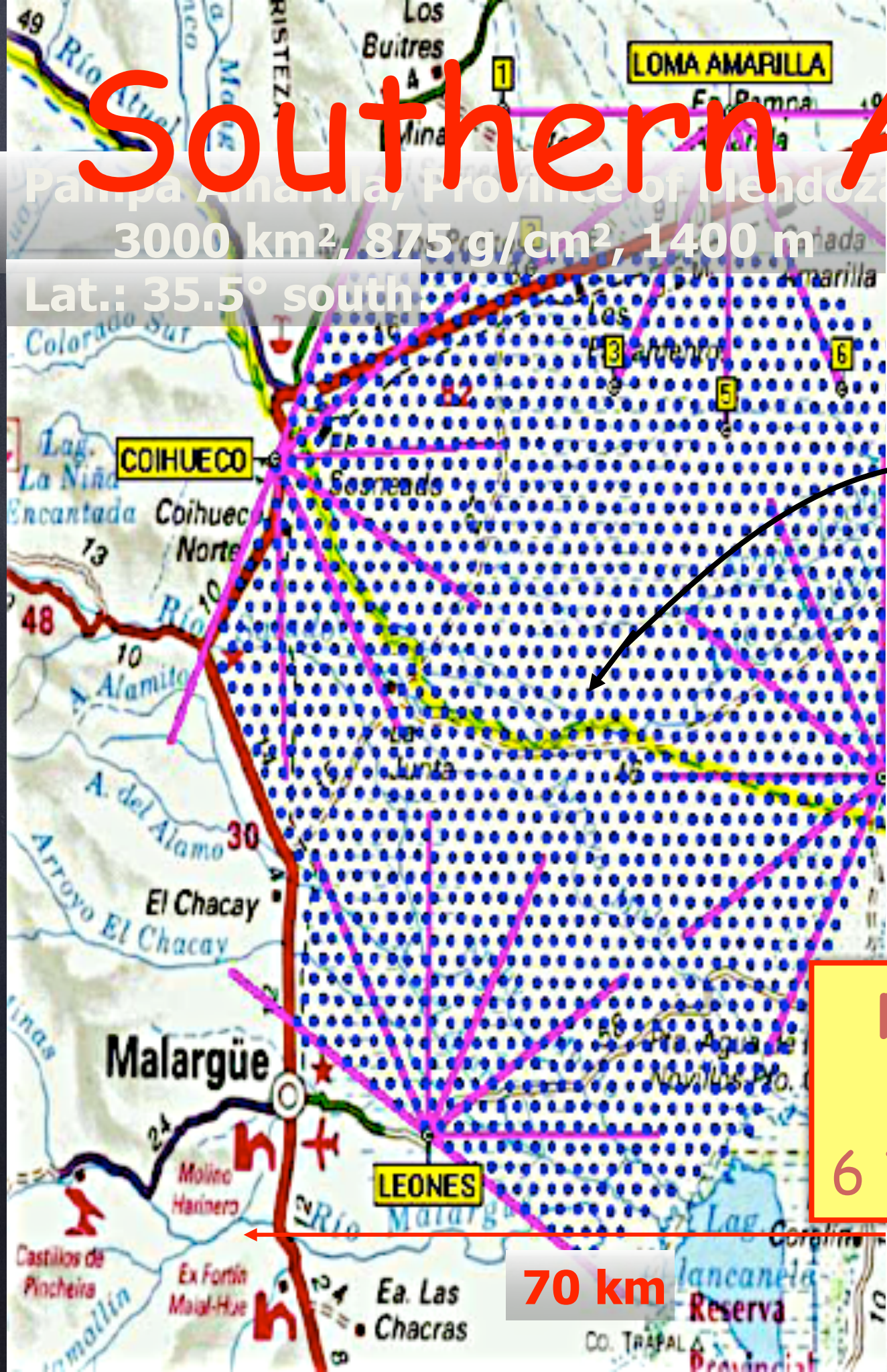


Southern Auger Site

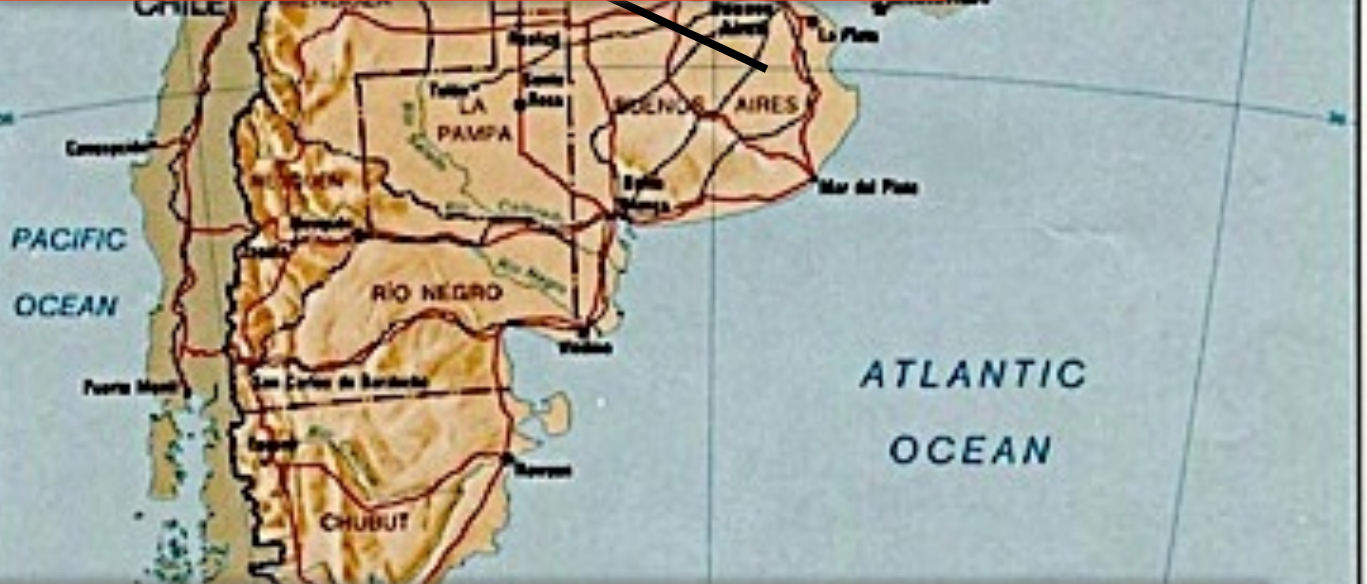
Pampa Amarilla, Province of Mendoza

3000 km², 875 g/cm², 1400 m

Lat.: 35.5° south

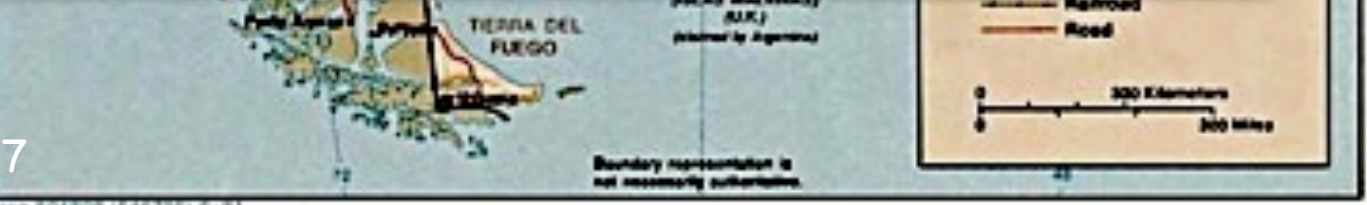


Surface Array (SD):
1600 Water Tanks
1.5 km spacing
3000 km²

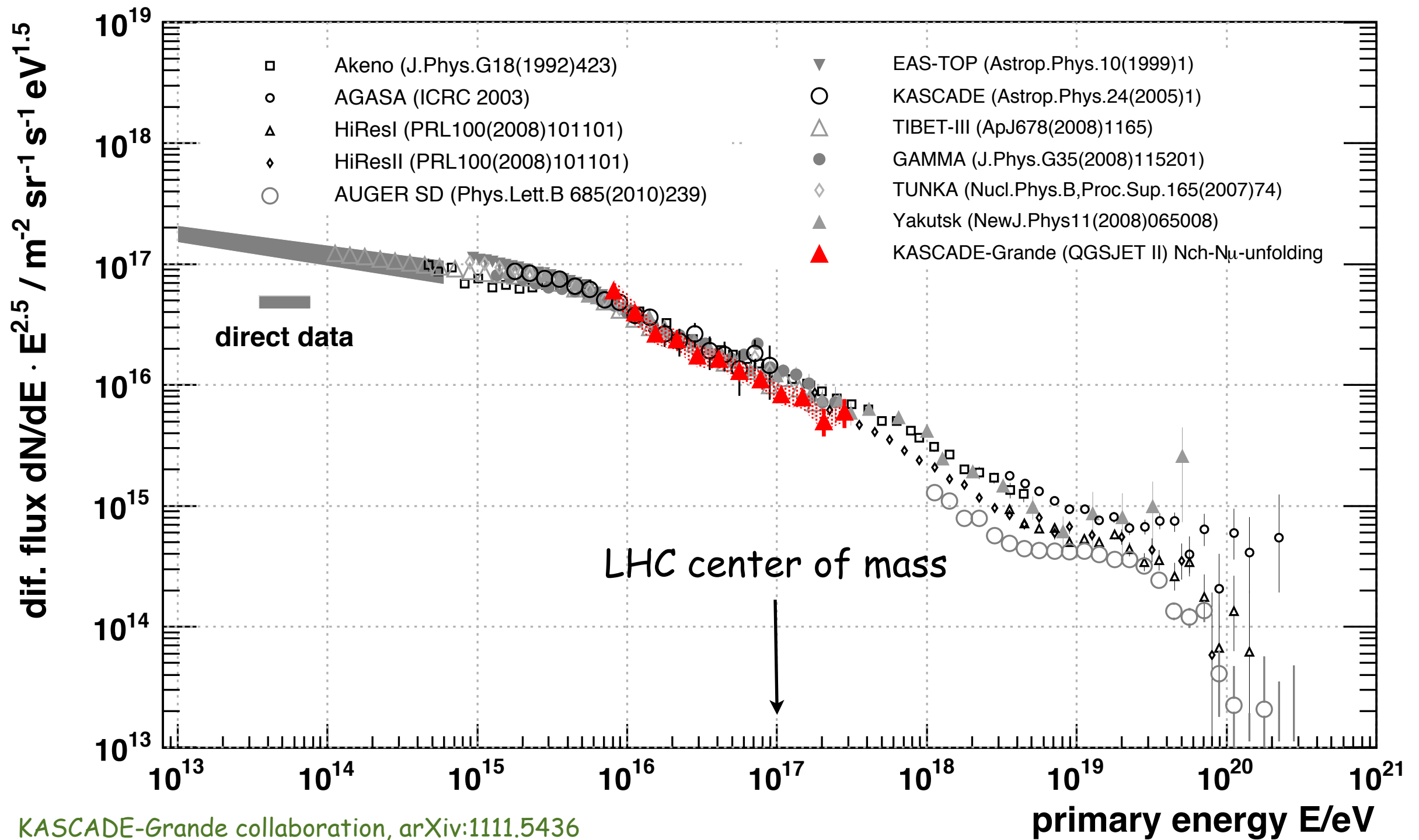


Fluorescence Detectors (FD):
4 Sites ("Eyes")
6 Telescopes per site (180° x 30°)

70 km



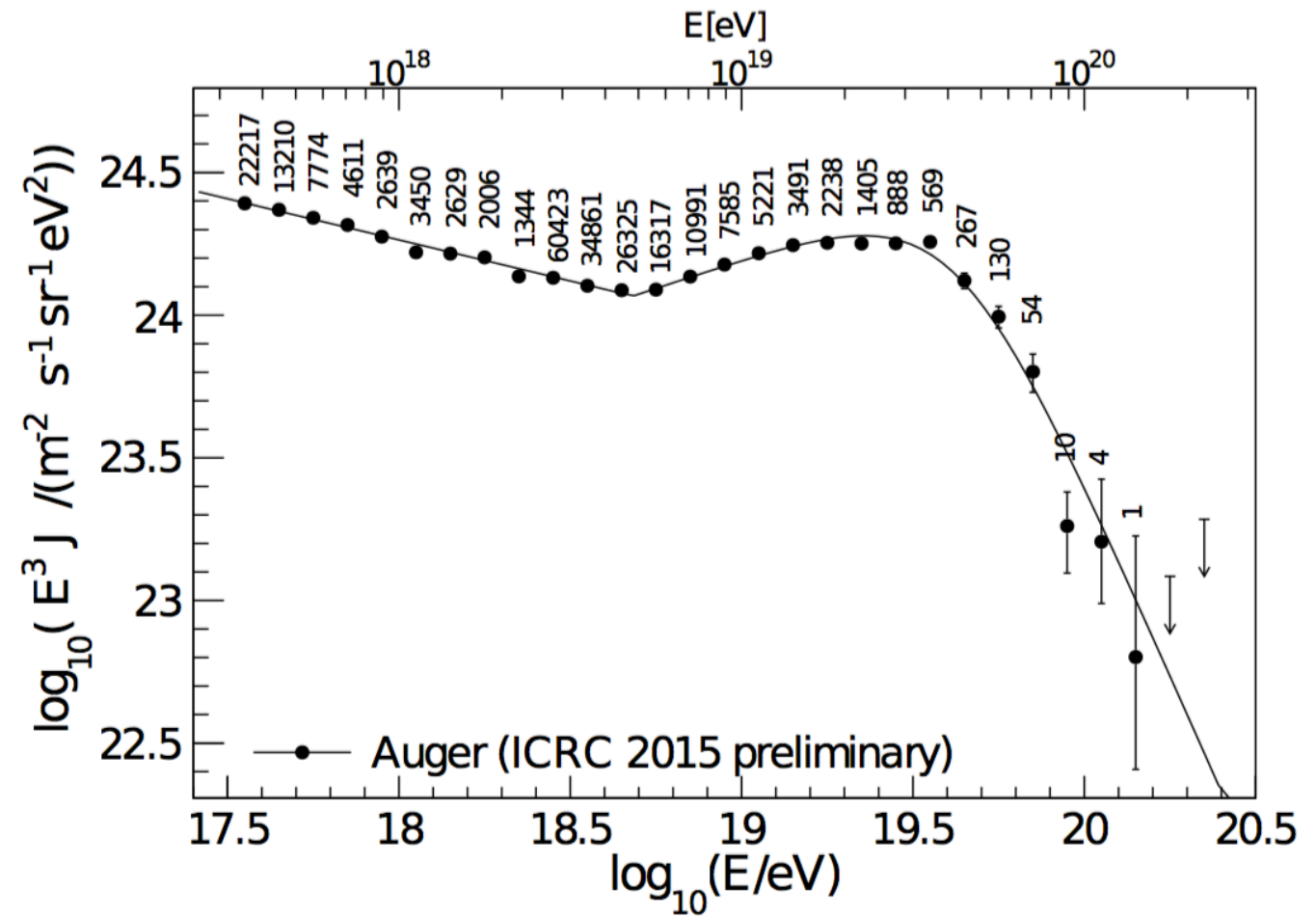
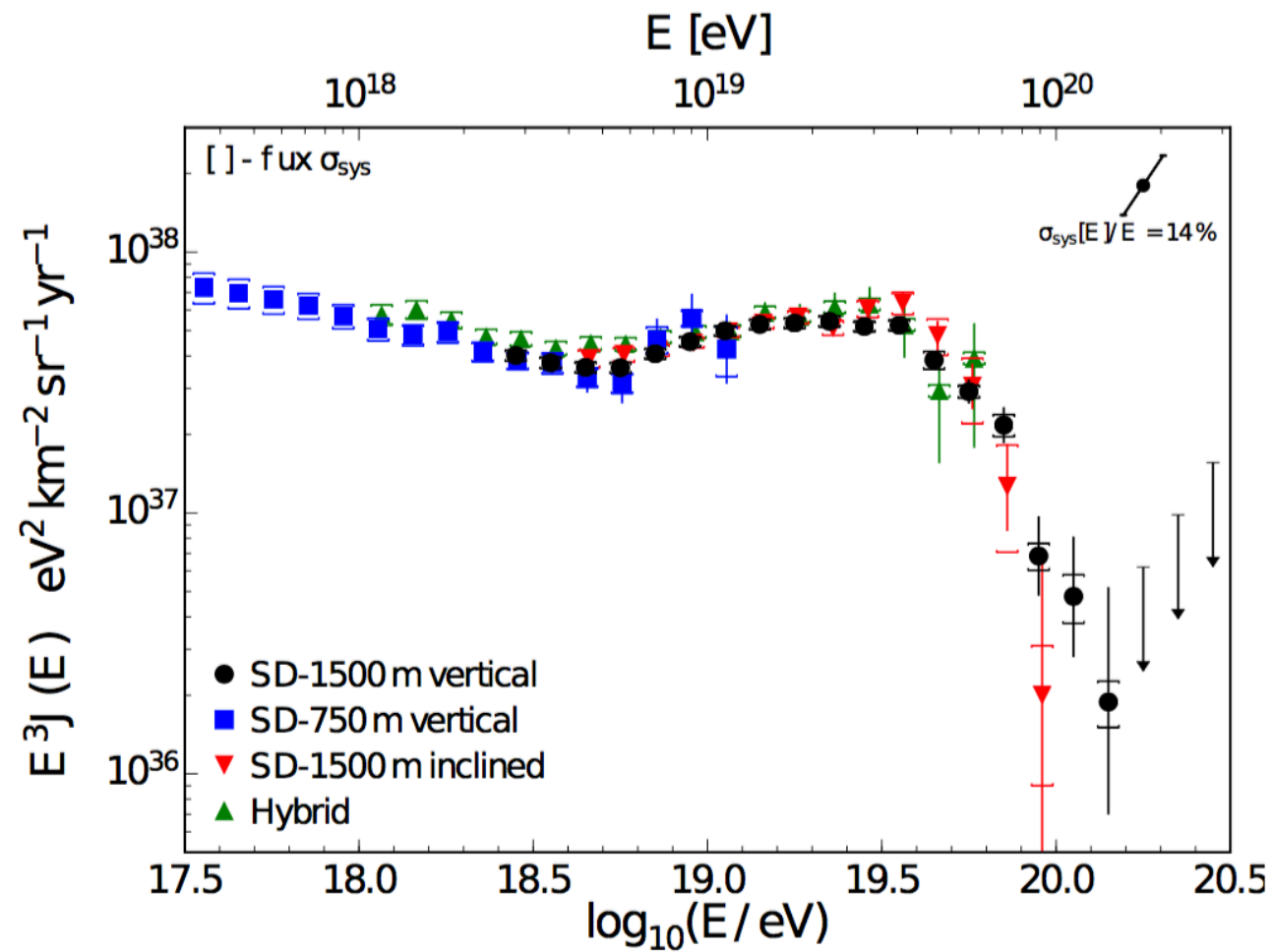
The All Particle Cosmic Ray Spectrum



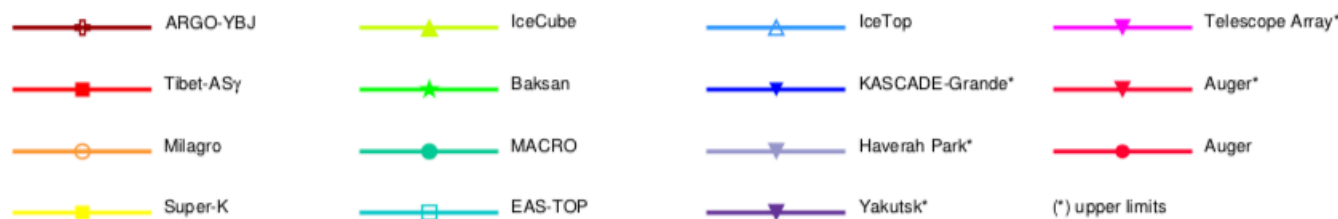
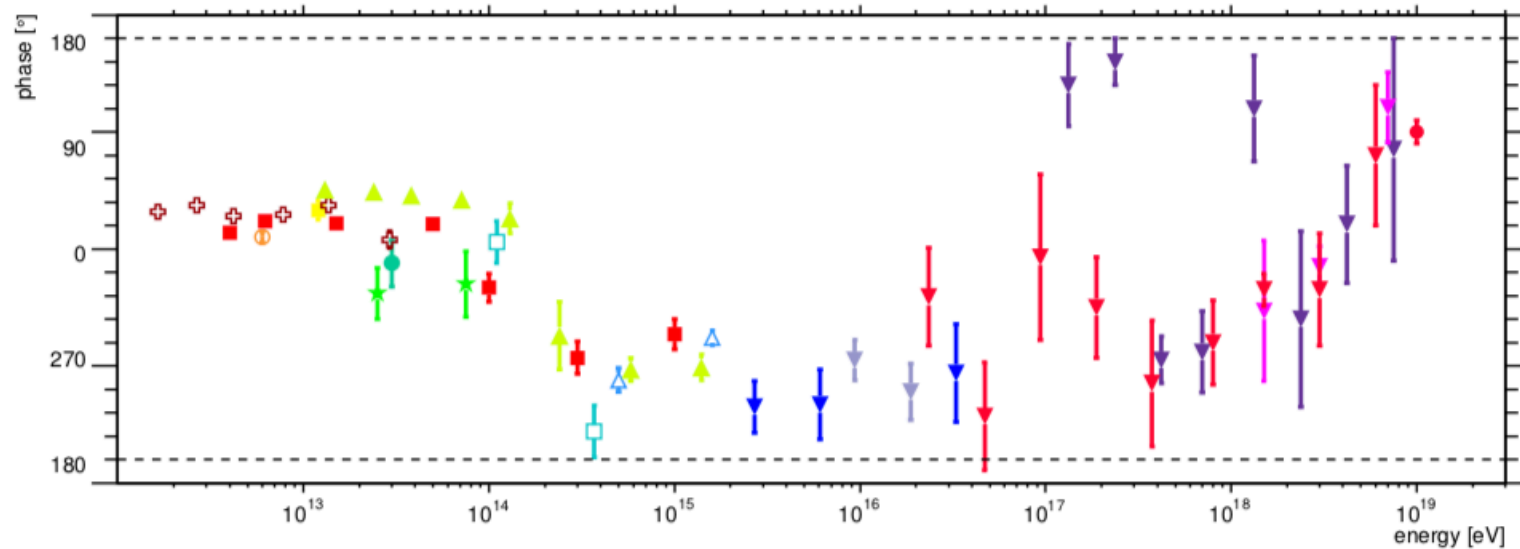
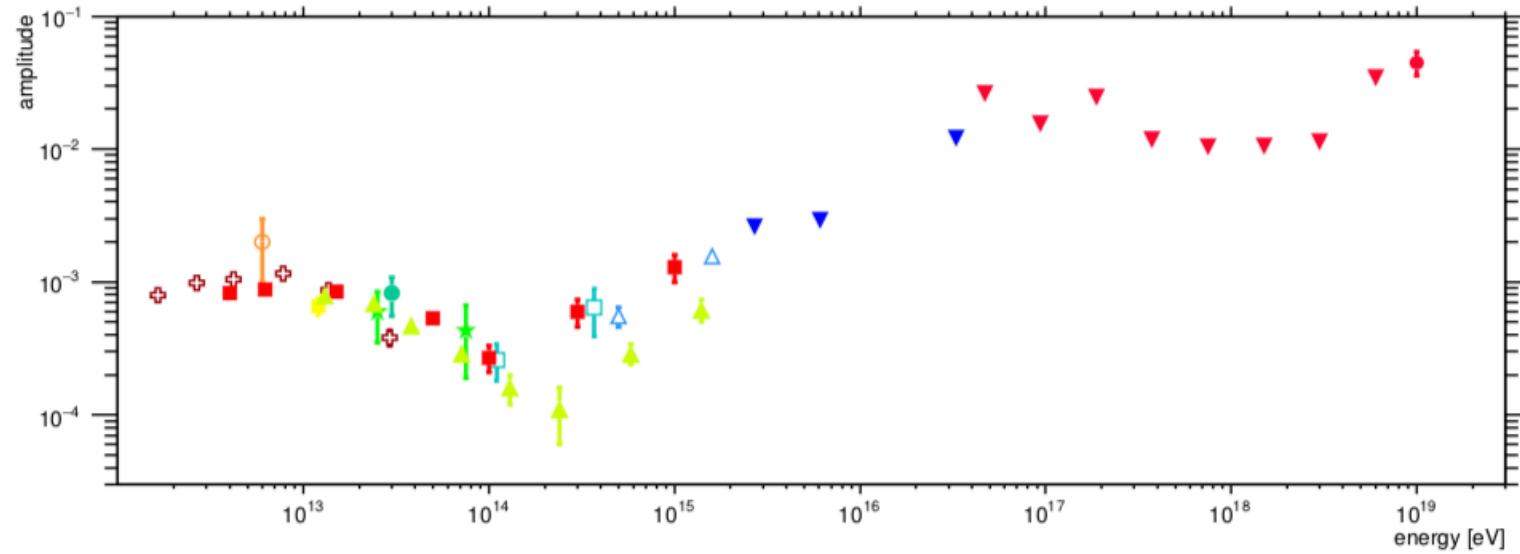
Pierre Auger Spectra

Auger exposure = 50000 km² sr yr, 102901 events above 3x10¹⁸ eV until end 2014

Pierre Auger Collaboration, PRL 101, 061101 (2008)
and Phys.Lett.B 685 (2010) 239
ICRC 2015, arXiv:1509.03732



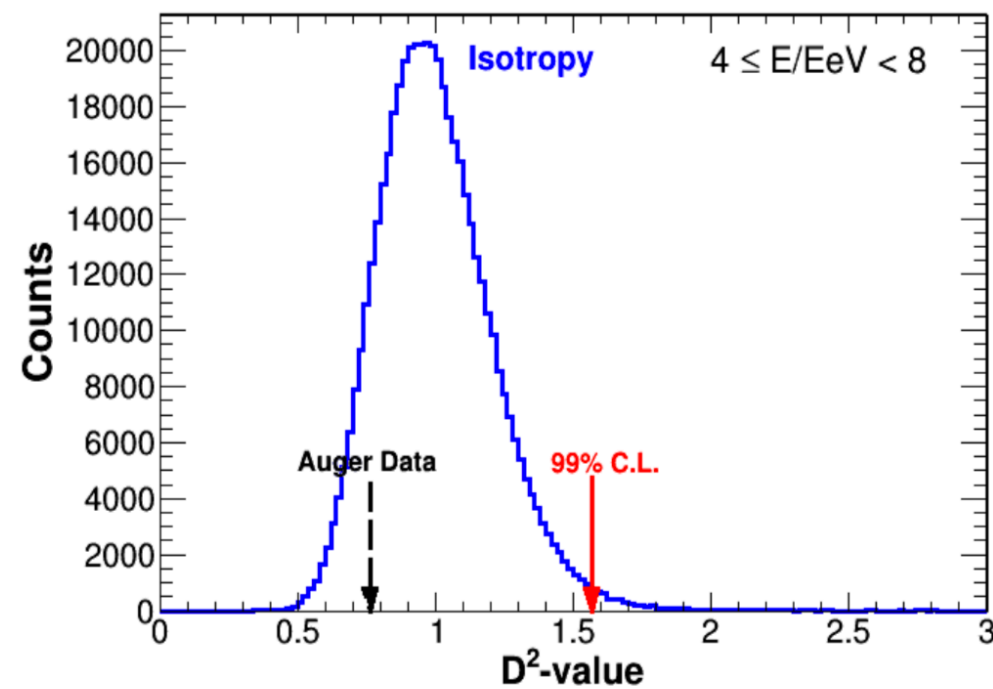
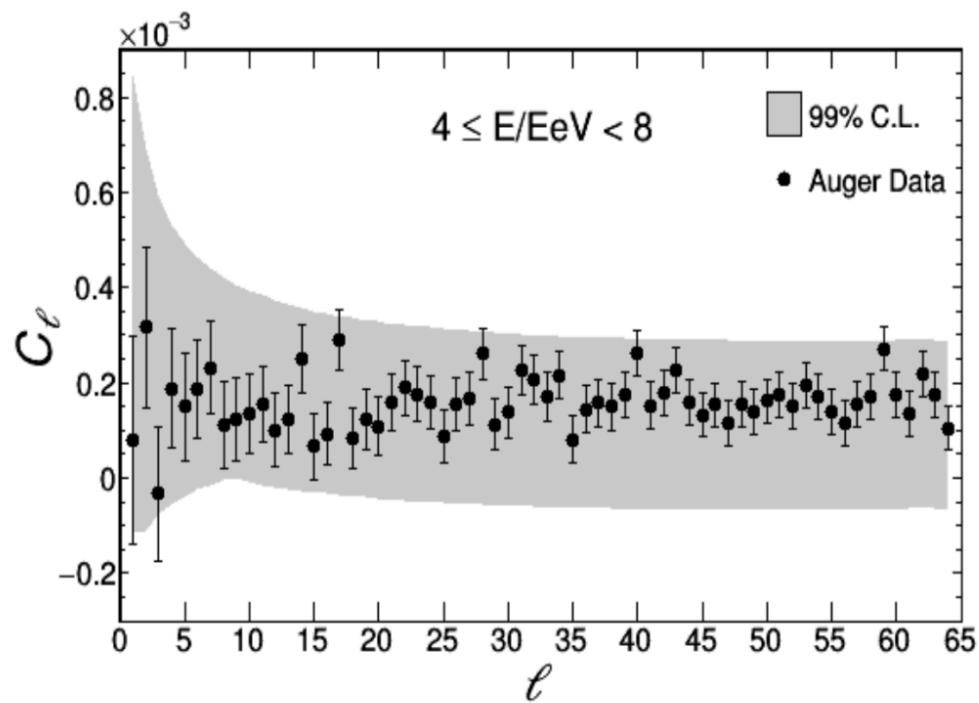
Newest Results on Anisotropy



Amplitude and phase of dipole as function of energy

O. Deligny, arXiv:1808.03940

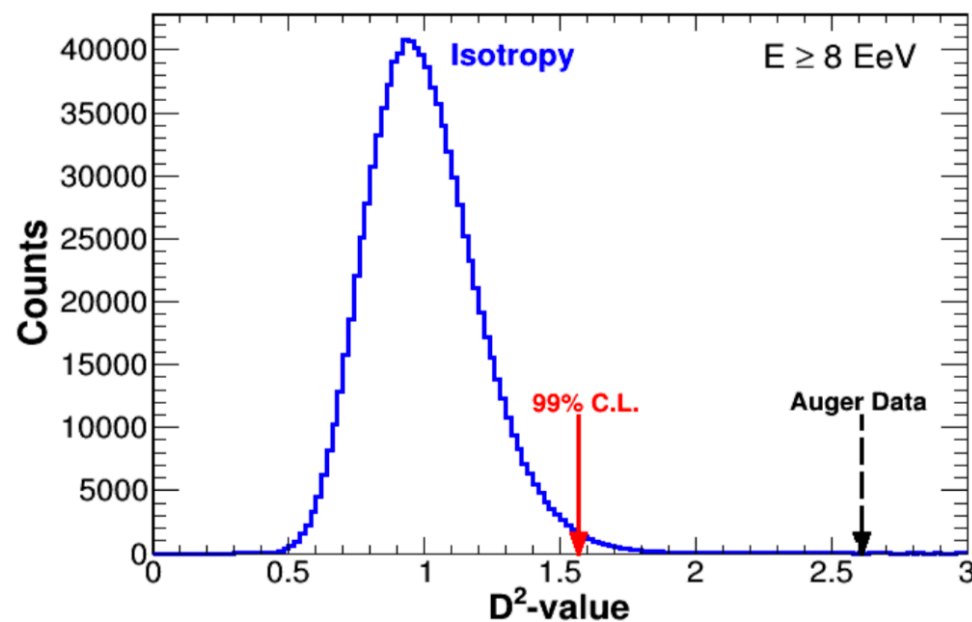
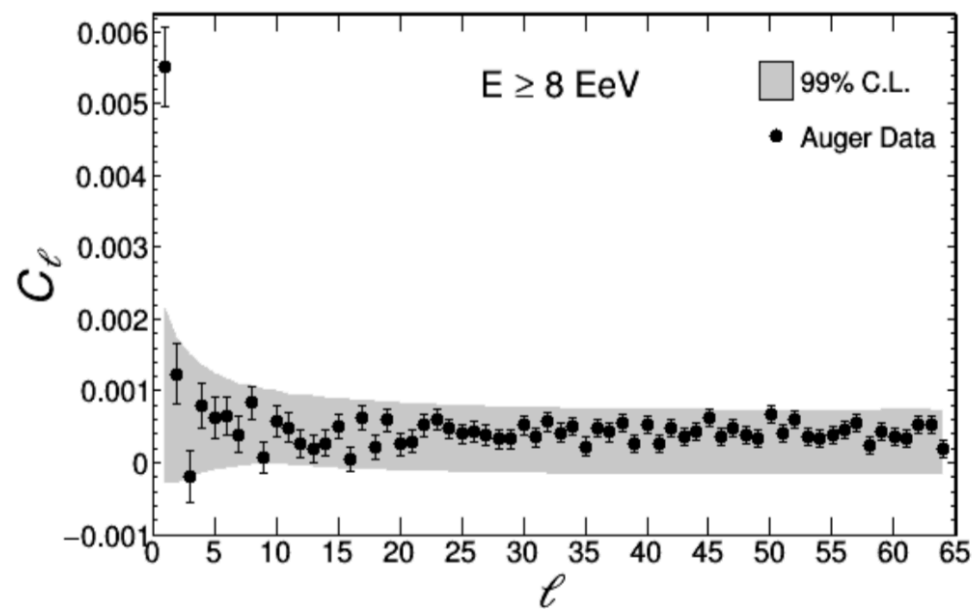
Figure 7: Amplitude (top) and phase (bottom) measurements of the first harmonic in right ascension as a function of energy, from various reports. Amplitudes drawn as triangles with apex pointing down are the most stringent upper limits up to date in the considered energy ranges.



higher order multipoles will become more important to model

Figure 2: Angular power spectrum for $4 \leq E/\text{EeV} < 8$. On the left there is no visible departure from the isotropic expectation. On the right the D^2 -value distribution from 500,000 isotropic sky maps is shown. The red arrow represents the threshold to accept/reject the isotropy hypothesis with 99% C.L..

The D^2 -value from data, represented by the black (dashed) arrow, is smaller than that threshold supporting the isotropy hypothesis.



Pierre Auger collaboration,
JCAP 1706 (2017) no.06,
026 [arXiv:1611.06812]

Figure 3: Angular power spectrum for $E \geq 8 \text{ EeV}$. On the left a clear indication for a departure from isotropy is captured in the dipole scale. On the right the D^2 -value distribution from 1,000,000 isotropic sky maps is shown. The D^2 -value from data, represented by the black (dashed) arrow, is larger than the threshold of isotropy presenting an indication of anisotropy with $> 99\%$ C.L..

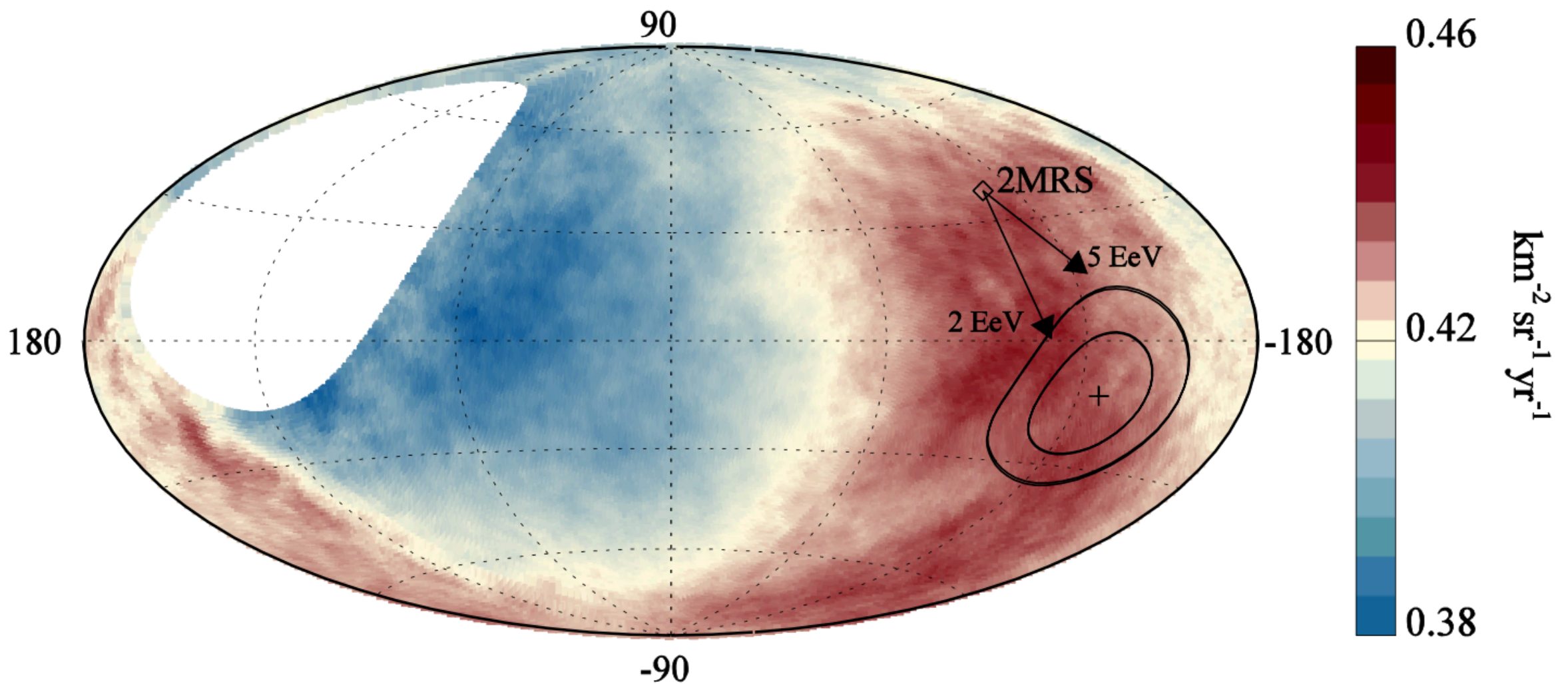


Fig. 3. Map showing the fluxes of particles in Galactic coordinates. Sky map in Galactic coordinates showing the cosmic-ray flux for $E \geq 8$ EeV smoothed with a 45° top-hat function. The Galactic center is at the origin. The cross indicates the measured dipole direction and the contours the 68% and 95% confidence-level regions. The dipole in the 2MRS galaxy distribution is indicated, while arrows show the deflections expected for a particular model of the Galactic magnetic field (8), for $E/Z=5$ EeV or 2 EeV.

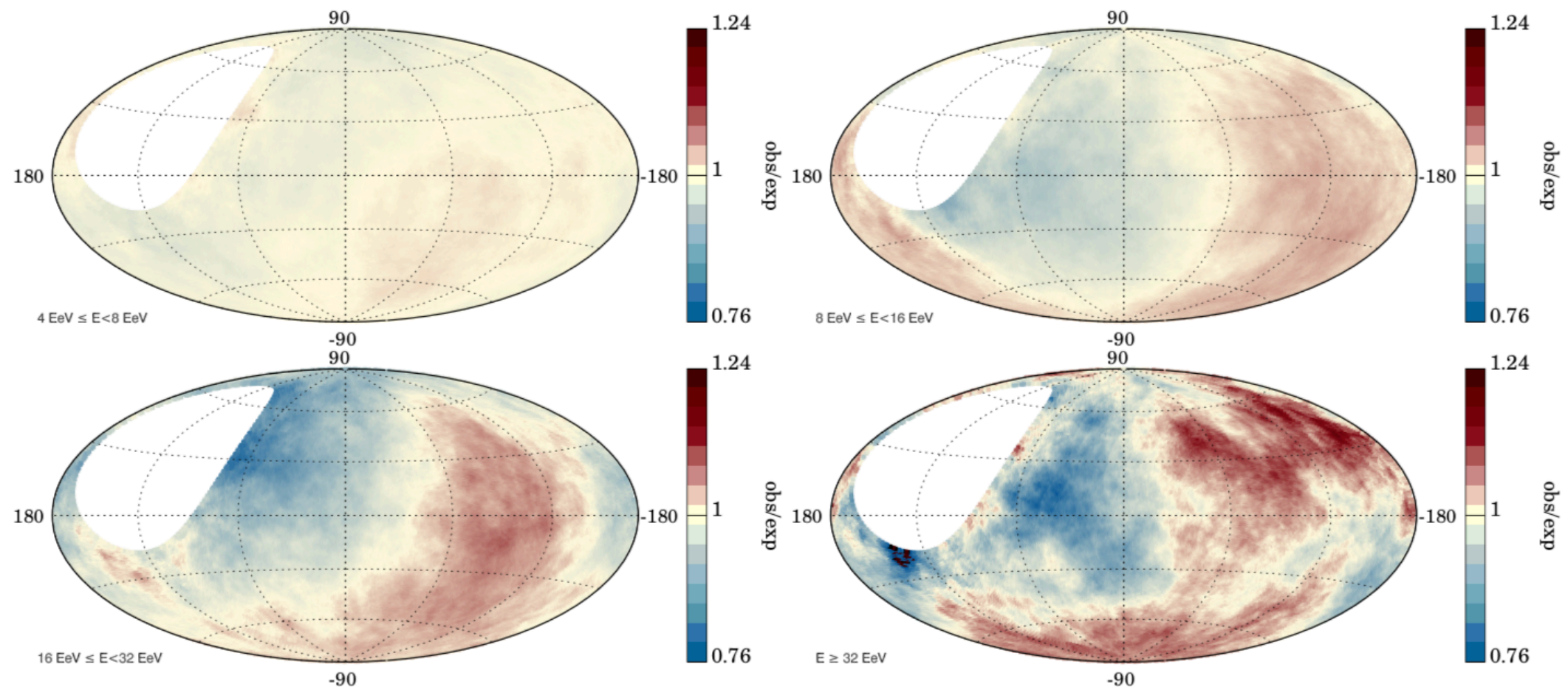


Figure 4. Maps in Galactic coordinates of the ratio between the number of observed events in windows of 45° over those expected for an isotropic distribution of arrival directions, for the four energy bins above 4 EeV.

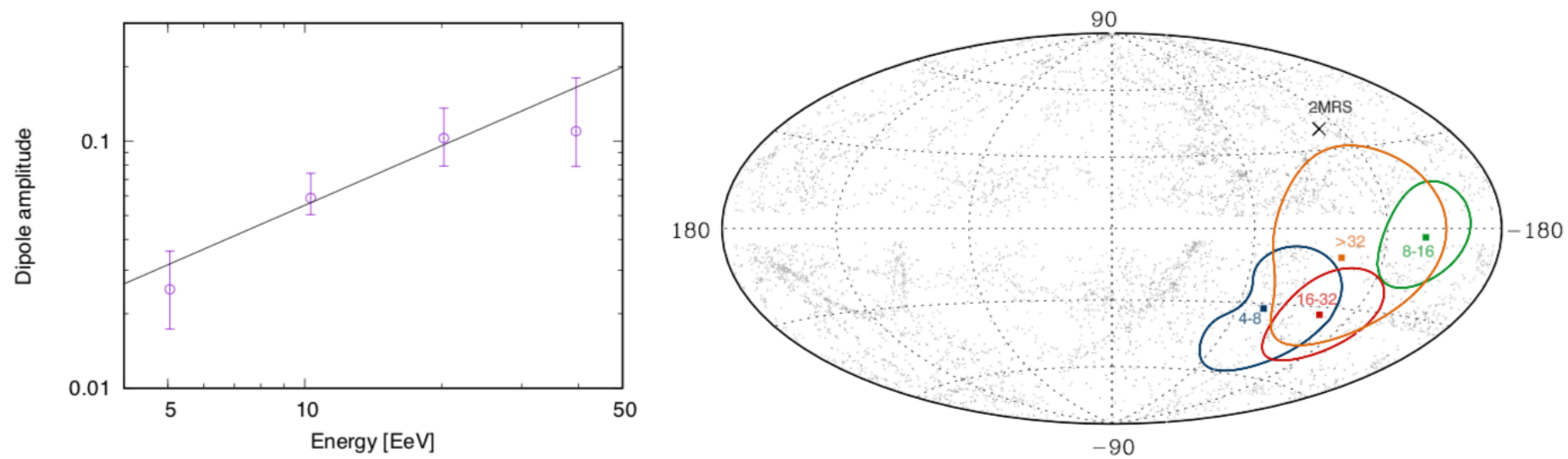


Figure 3. Evolution with energy of the amplitude (left panel) and direction (right panel) of the three-dimensional dipole determined in different energy bins above 4 EeV. In the sky map in Galactic coordinates of the right panel the dots represent the direction towards the galaxies in the 2MRS catalog that lie within 100 Mpc and the cross indicates the direction towards the flux-weighted dipole inferred from that catalog.

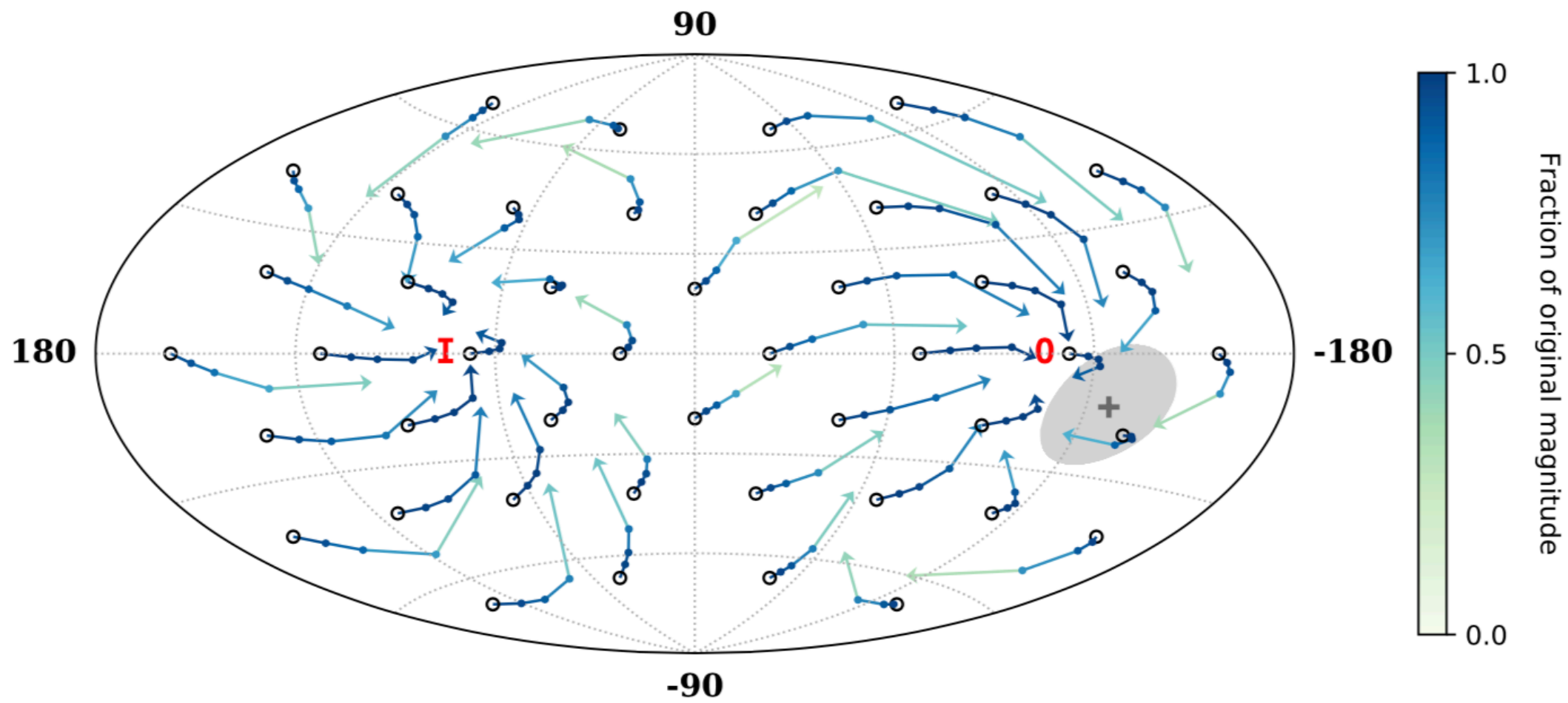
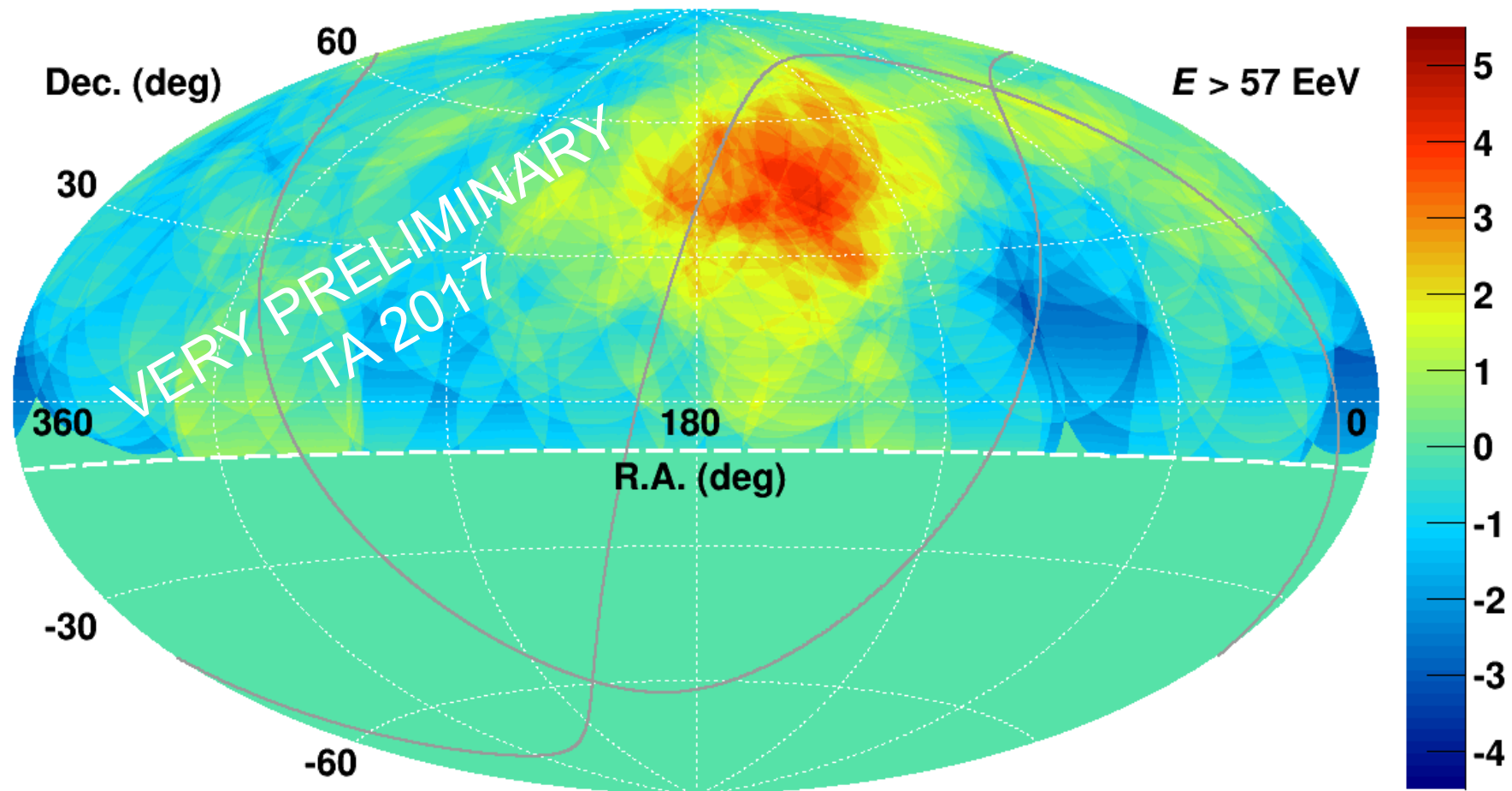


Figure 7. Change of the direction of the dipolar component of an extragalactic flux after traversing the Galactic magnetic field, modeled as in [Jansson & Farrar \(2012\)](#). We consider a grid (black circles) corresponding to the directions of a purely dipolar flux outside the Galaxy. Points along the lines indicate the reconstructed directions for different values of the particle rigidity: 32 EV, 16 EV, 8 EV and, at the tip of the arrow, 4 EV, respectively. The line color indicates the resulting fractional change of the dipole amplitude. The observed direction of the dipole for energies $E \geq 8$ EeV is indicated by the gray cross, with the shaded area indicating the 68% CL region. The labels **I** and **O** indicate the directions towards the inner and outer spiral arms, respectively.

Hot spot

$E > 57$ EeV - Years 1-9 excess map



Total events: 143
Observed: 34
Expected : 13.5

Best circle center: RA=144.3°, Dec=+40.3°
Best circle radius: 25°
Local significance : 5 σ
Global significance : 3 σ

TA 2017



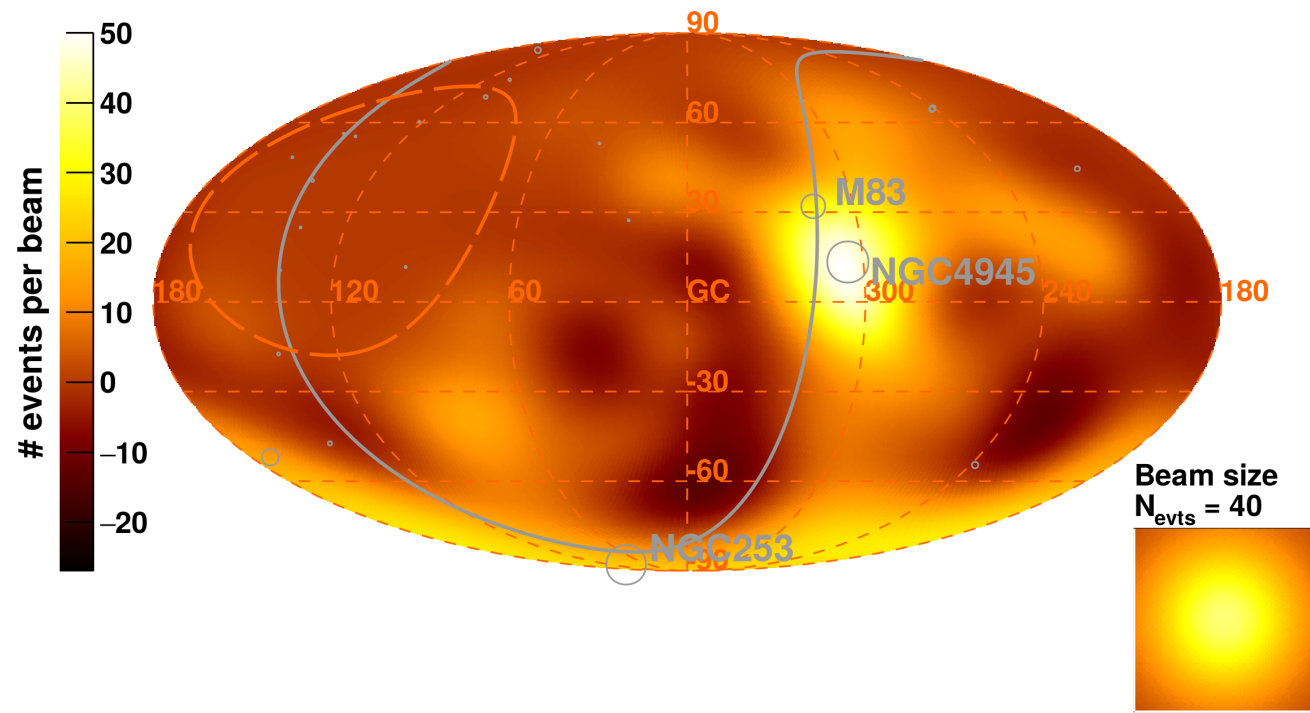
TA anisotropy//TeVPA2018

28.08.2018

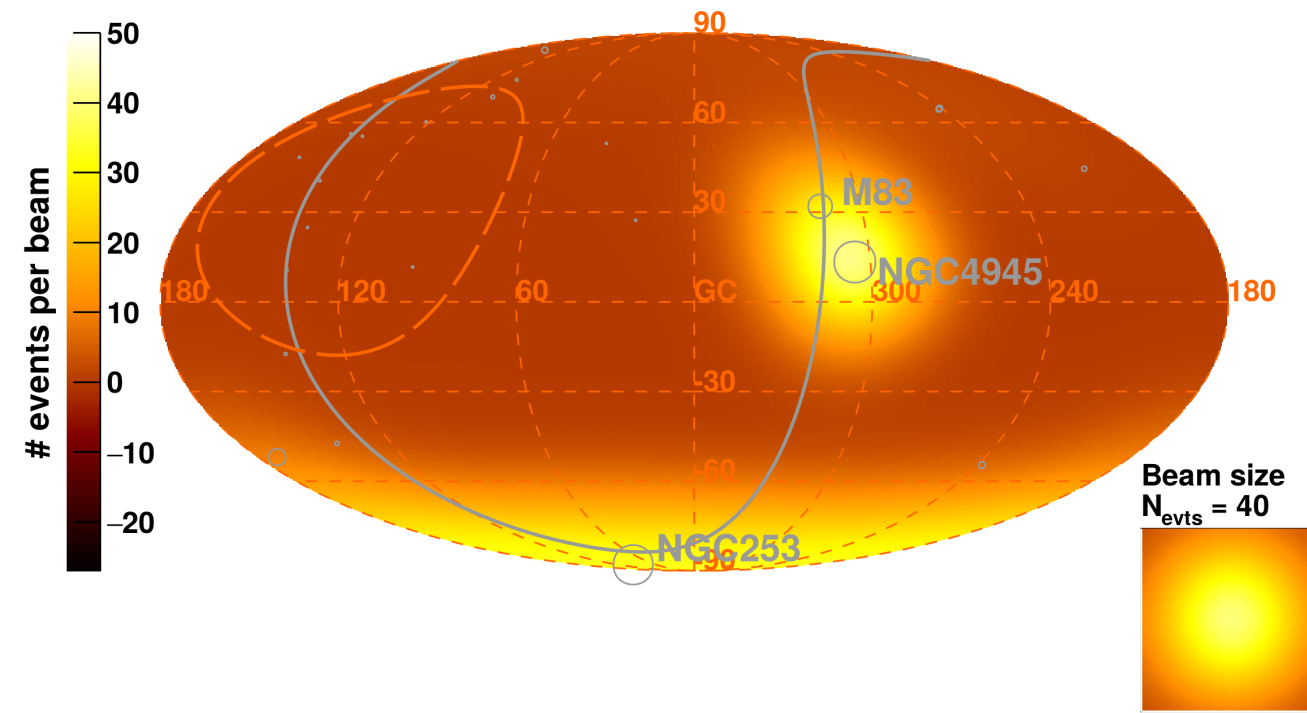
slide 7 of 17



Observed Excess Map - $E > 39$ EeV

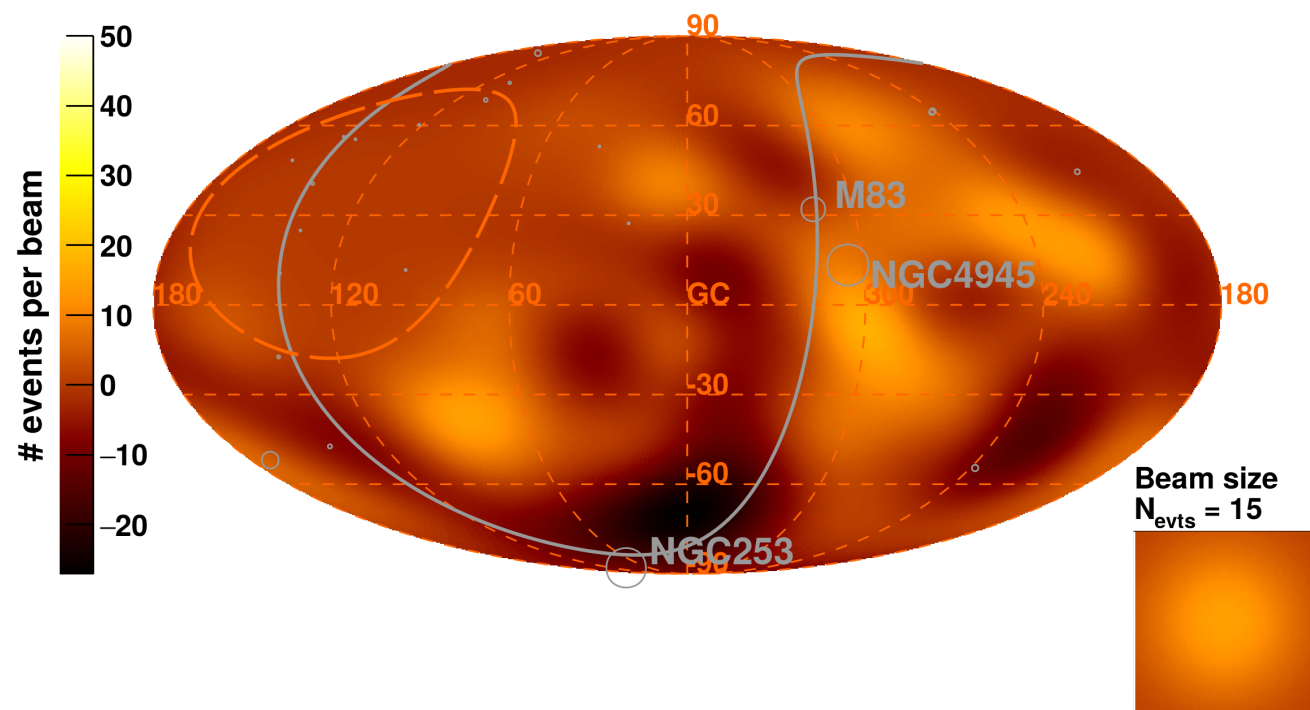


Model Excess Map - Starburst galaxies - $E > 39$ EeV



Pierre Auger collaboration, *Astrophys. J.* 853 (2018) no.2, L29 [arXiv:1801.06160]

Residual Excess Map - Starburst galaxies - $E > 39$ EeV



Model Flux Map - Starburst galaxies - $E > 39$ EeV

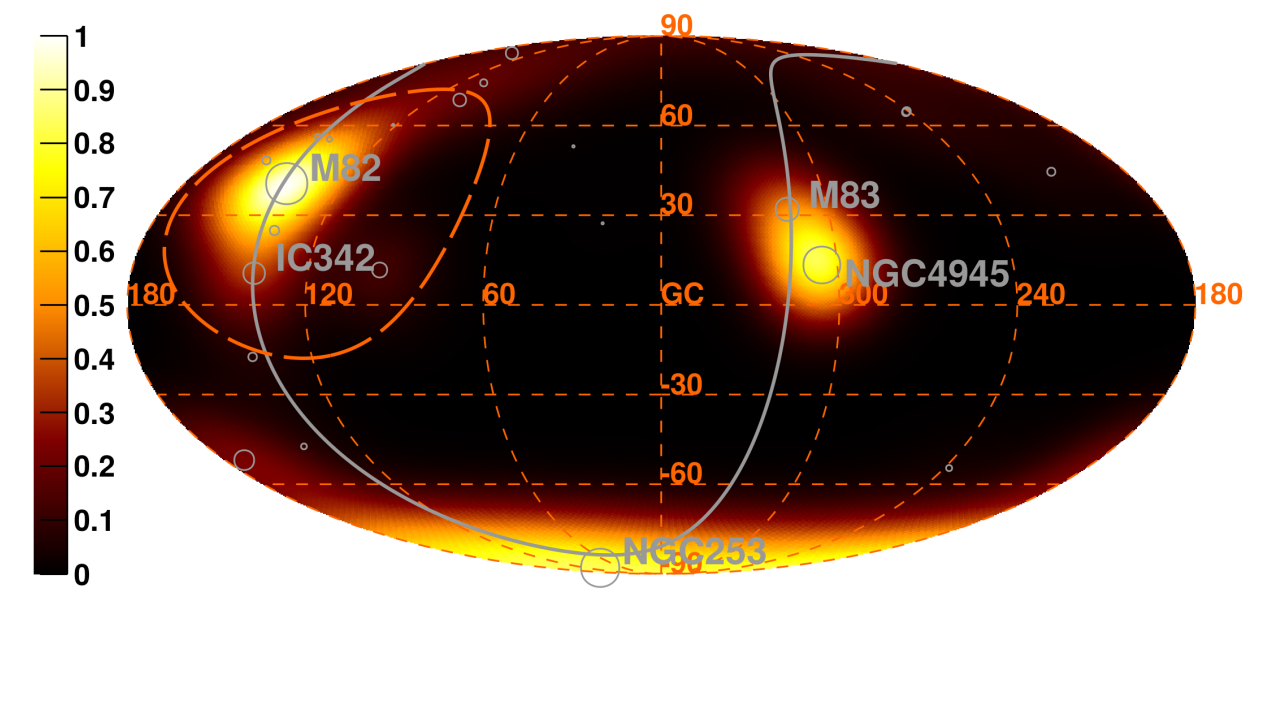
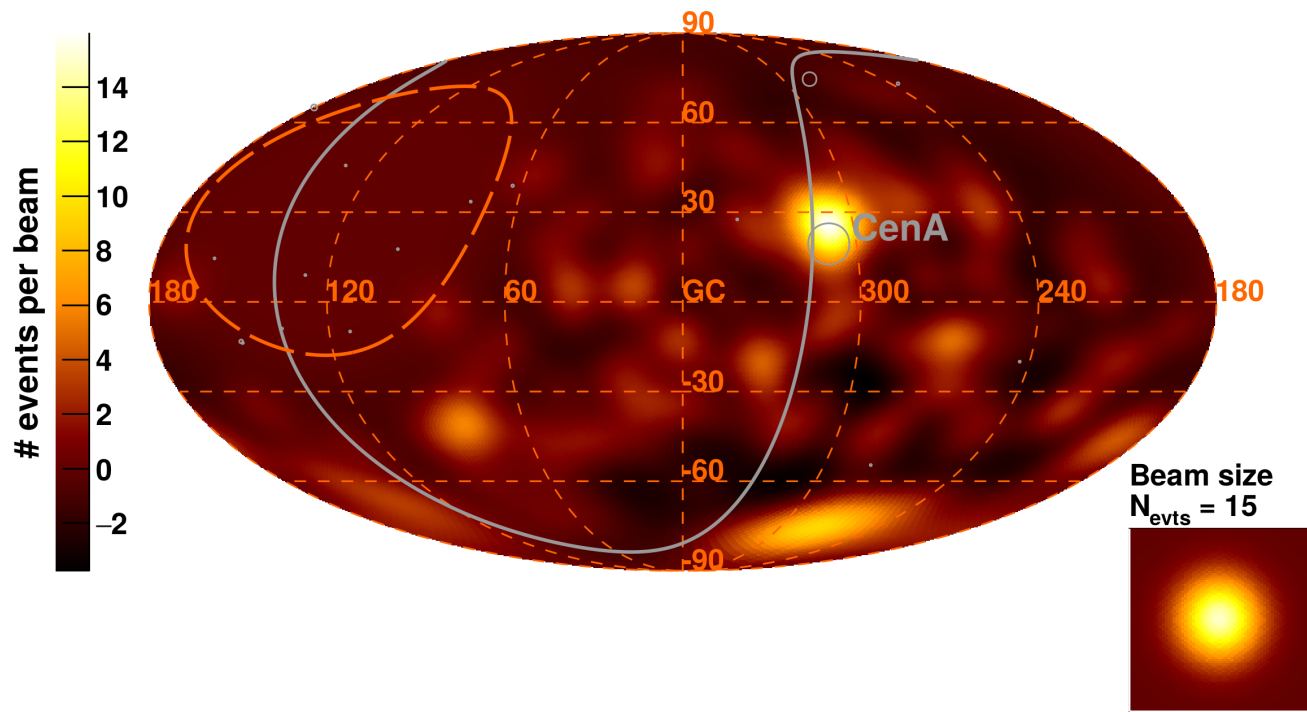
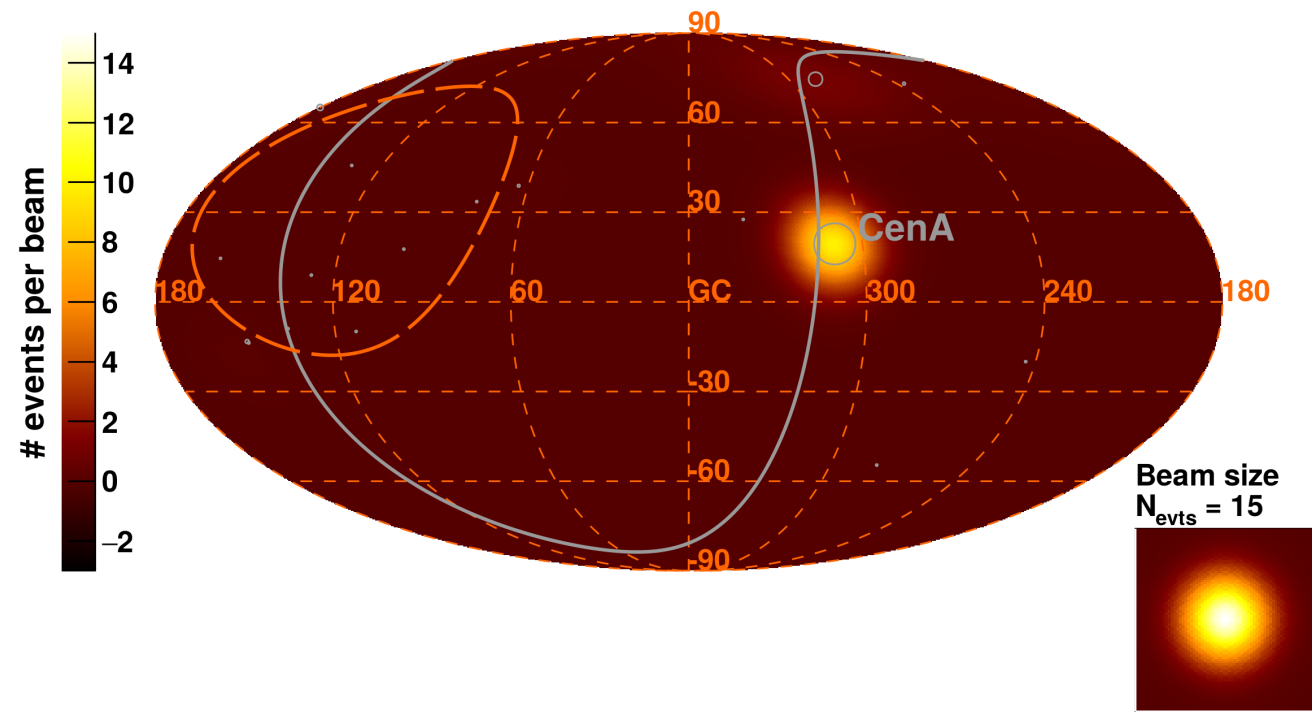


Figure 3. *Top to Bottom:* Observed excess map - Model excess map - Residual map - Model flux map, for the best-fit parameters obtained with SBGs above 39 EeV (*Left*) and γ AGNs above 60 EeV (*Right*). The excess maps (best-fit isotropic component subtracted) and residual maps (observed minus model) are smeared at the best-fit angular scale. The color scale indicates the number of events per smearing beam (see inset). The model flux map corresponds to a uniform full-sky exposure. The supergalactic plane is shown as a solid gray line. An orange dashed line delimits the field of view of the array.

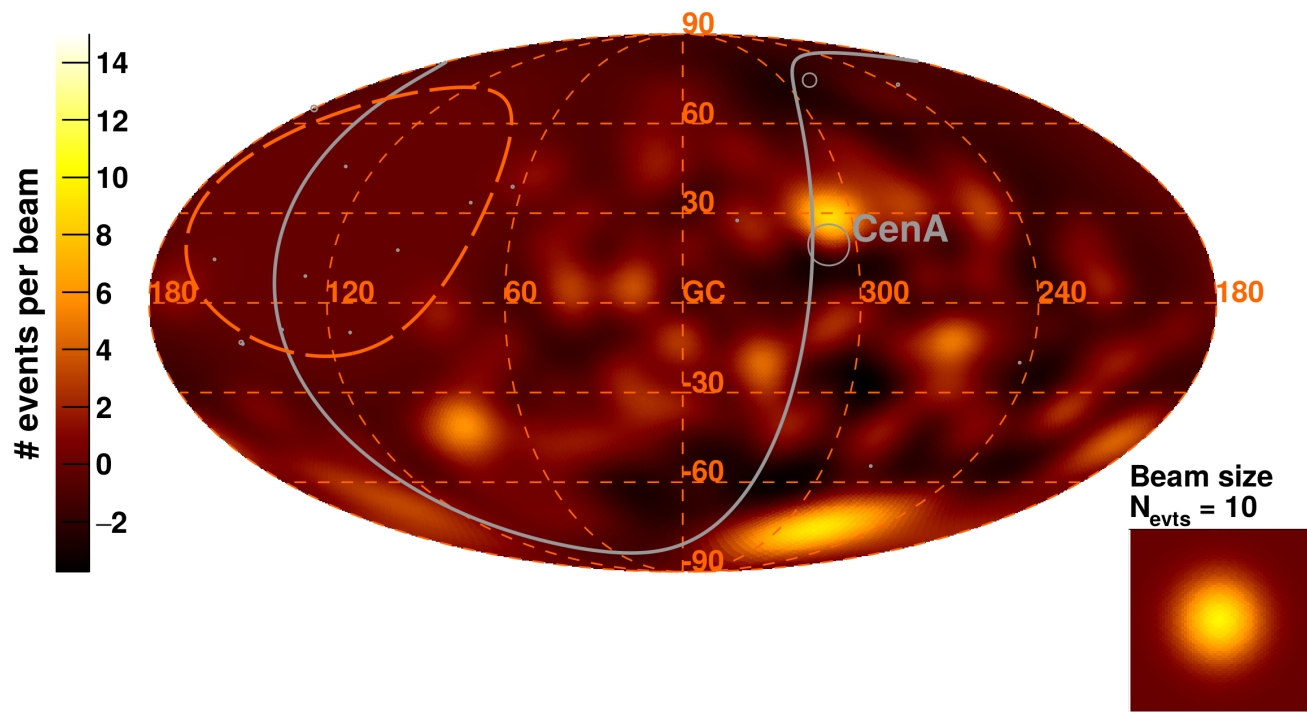
Observed Excess Map - $E > 60$ EeV



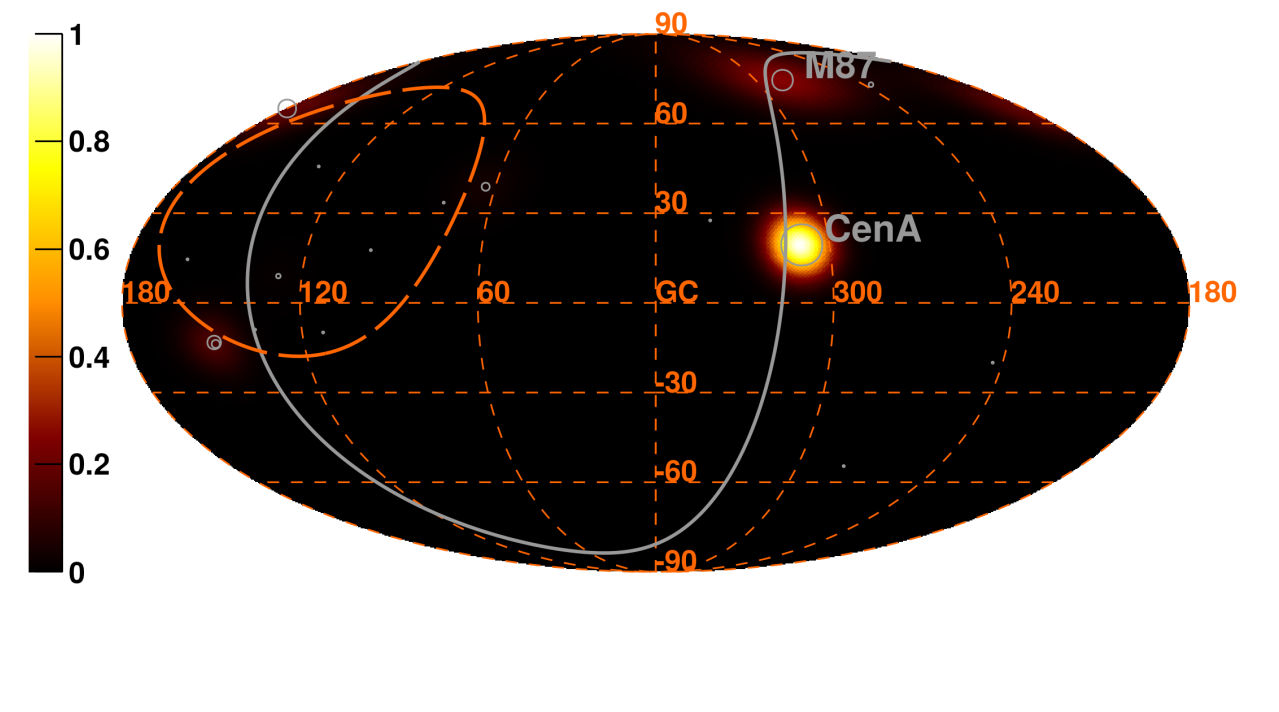
Model Excess Map - Active galactic nuclei - $E > 60$ EeV

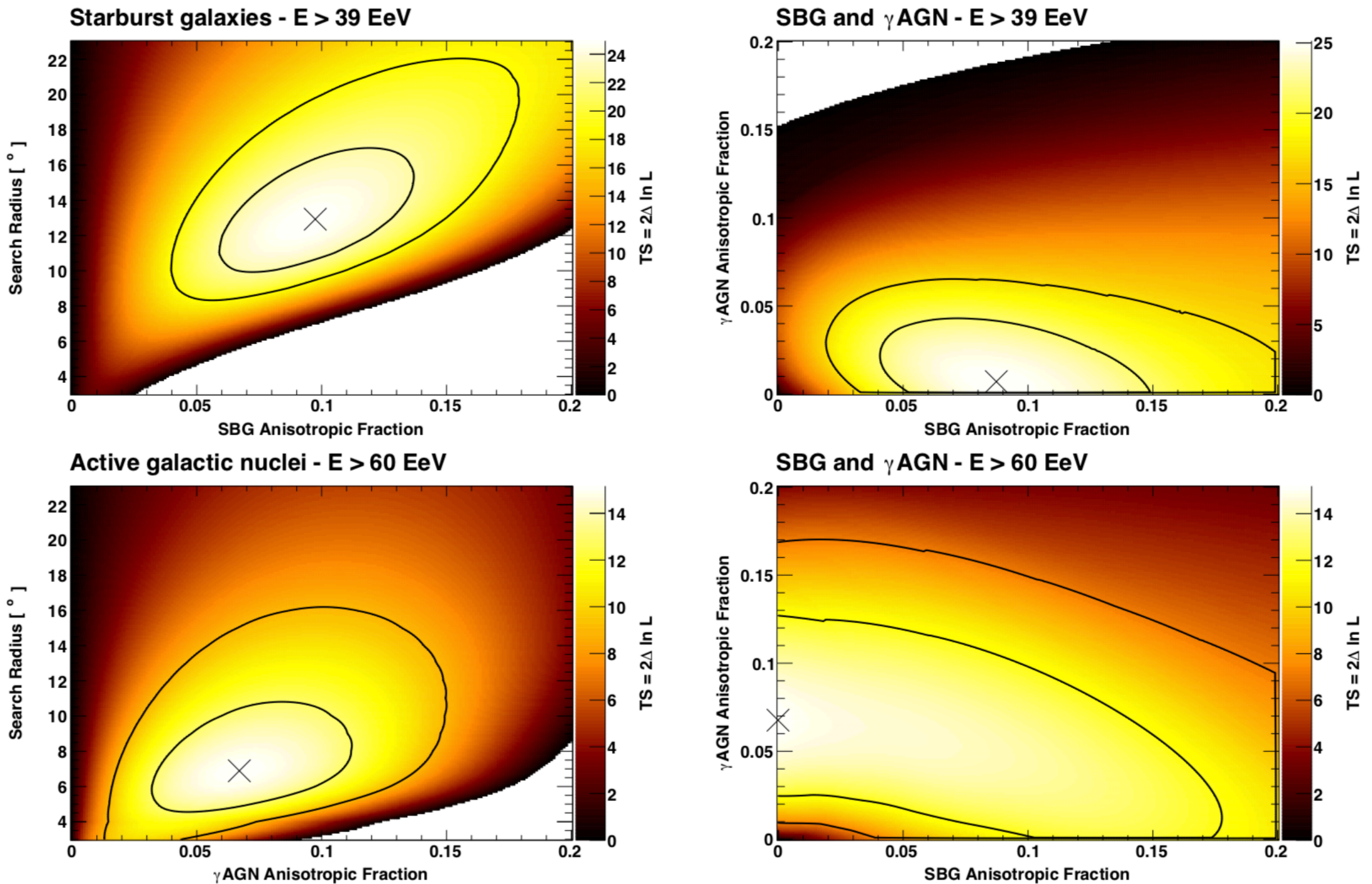


Residual Excess Map - Active galactic nuclei - $E > 60$ EeV



Model Flux Map - Active galactic nuclei - $E > 60$ EeV





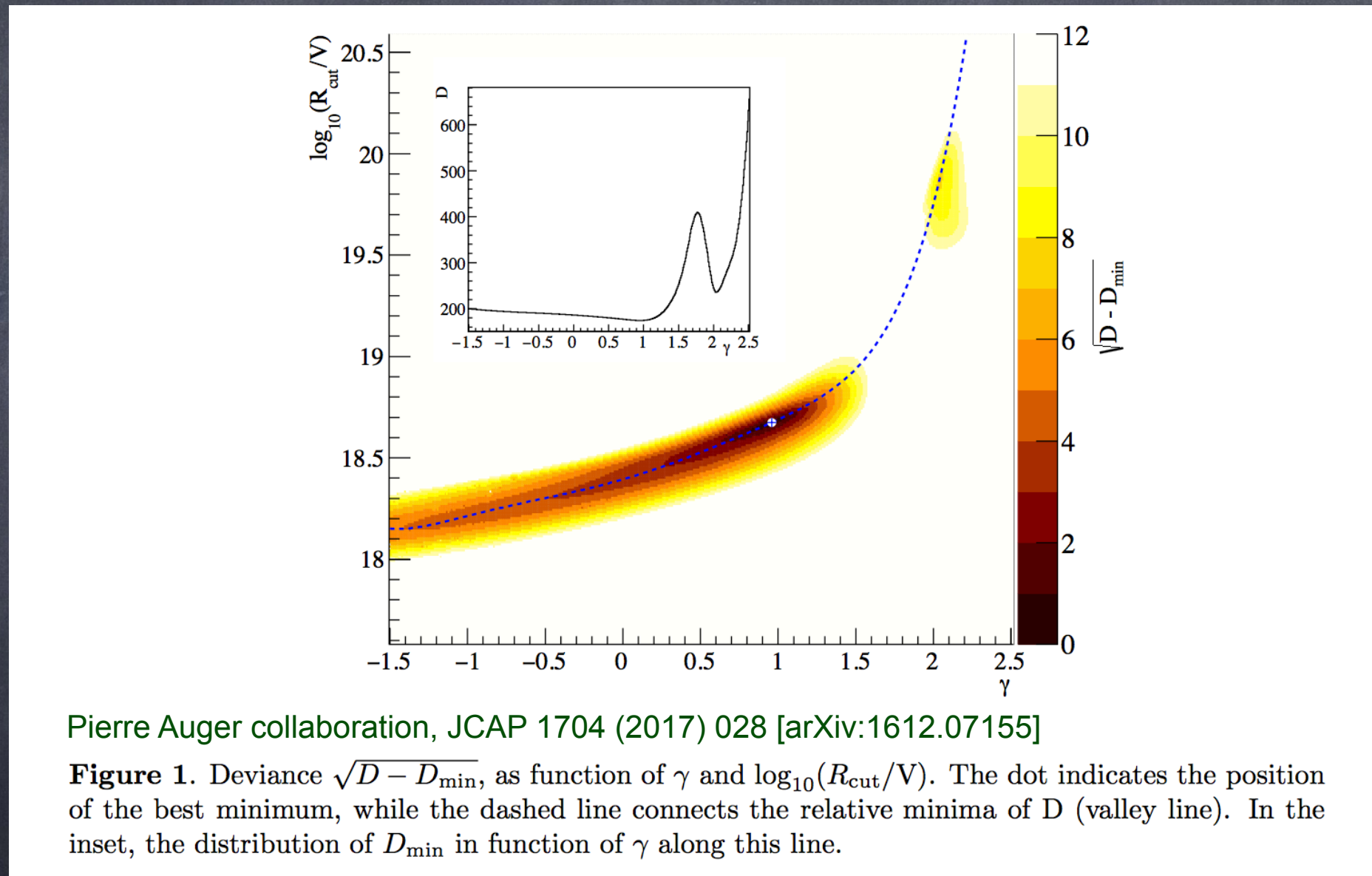
Pierre Auger collaboration, *Astrophys. J.* 853 (2018) no.2, L29 [arXiv:1801.06160]

Figure 2. TS profile above 39EeV (Top) and 60EeV (Bottom) over the fit parameters for SBG-only and γ AGN-only models (Left) and for composite models including both SBGs and γ AGNs with the same free search radius (Right). The lines indicate the 1–2 σ regions.

The strongest signal of about 4 sigma occurs for starburst galaxies above ~ 39 EeV (correlating fraction $\sim 10\%$ and correlation angle 12-14 degrees).

Spectrum and Composition

fits to spectrum and composition for a homogeneous source distribution neglecting deflection (which generally is a good approximation for the solid angle integrated flux) tend to favor very hard injection spectra with low cut-off rigidities



comparatively low cutoff may be mostly caused by source physics; Peters cycle at highest energies is most "economic" in terms of source power

Some General Considerations

Reminder: Propagation Theorem/Liouville Theorem

A homogeneous distribution of sources with equal properties and nearest neighbour distances smaller than other relevant length scales in the problem such as energy loss length and propagation/diffusion length within the source activity time scale gives rise to a universal/isotropic flux spectrum that does not depend on the propagation mode and thus on the magnetic field properties.

Easiest to see in the back-tracking picture:

The differential flux in the direction characterised by the unit vector \mathbf{n} at observer position \mathbf{r}_0 is given by

$$j(E_0, \mathbf{r}_0, \mathbf{n}) = \int_{t_0}^{t_{\max}} dt \dot{\rho} [E(t), t, \mathbf{r}(t, \mathbf{n})] ,$$

where $\dot{\rho}(E, t, \mathbf{r})$ is the differential injection rate at energy E , time t , and location \mathbf{r} , $\mathbf{r}(t, \mathbf{n})$ is the back-tracked trajectory with the initial conditions $\mathbf{r}(t_0, \mathbf{n}) = \mathbf{r}_0$, $\dot{\mathbf{r}}(t_0, \mathbf{n}) = \mathbf{n}$ and $E(t)$ with $E(t_0) = E_0$ is the back-tracked energy. For stochastic losses one has to average over trajectories with equal initial conditions.

Clearly, if $\dot{\rho}$ only depends on E and t , then the flux neither depends on the shape of the trajectories nor on direction, but only on energy, and thus is universal.

This also applies to secondary fluxes such as neutrinos and gamma-rays because densities only depend on the time-integrated interaction rates (and energy loss rates) which are location independent

Corollary:

To be sensitive to the propagation mode, magnetic field structure etc. requires discrete, inhomogeneous source distributions with nearest-neighbour distances larger than energy loss length and/or propagation distance within source activity time

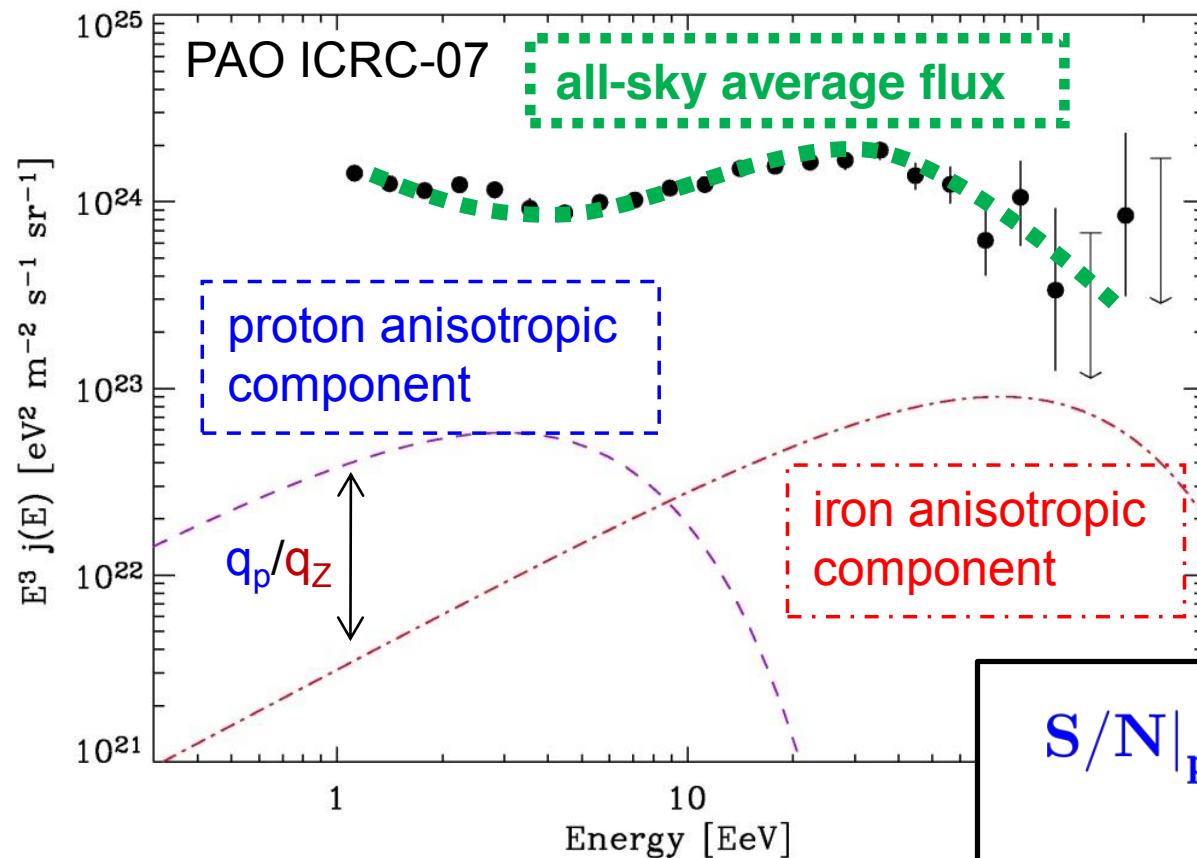
Modelling Challenges

- Broad dynamic range in length and time scales
- partly unknown propagation mode: ballistic versus diffusive
- disentangling source distribution/rates from propagation mode

Anisotropies vs heavy composition at UHE



→ if anisotropic signal $>E$ is due to heavy nuclei, one should detect a **stronger anisotropy signal associated with protons of same magnetic rigidity at $>E/Z$ eV...**
argument independent of intervening magnetic fields... (M.L. & Waxman 09, Liu+13)



Compare strength of anisotropy at E and E/Z :

$$S/N|_p (> E/Z) \simeq \underbrace{\alpha_{\text{loss},Z}}_{>1} \underbrace{Z^{-0.85}}_{<1} \underbrace{\frac{N_p}{N_Z}}_{\gg 1} S/N|_Z (> E)$$

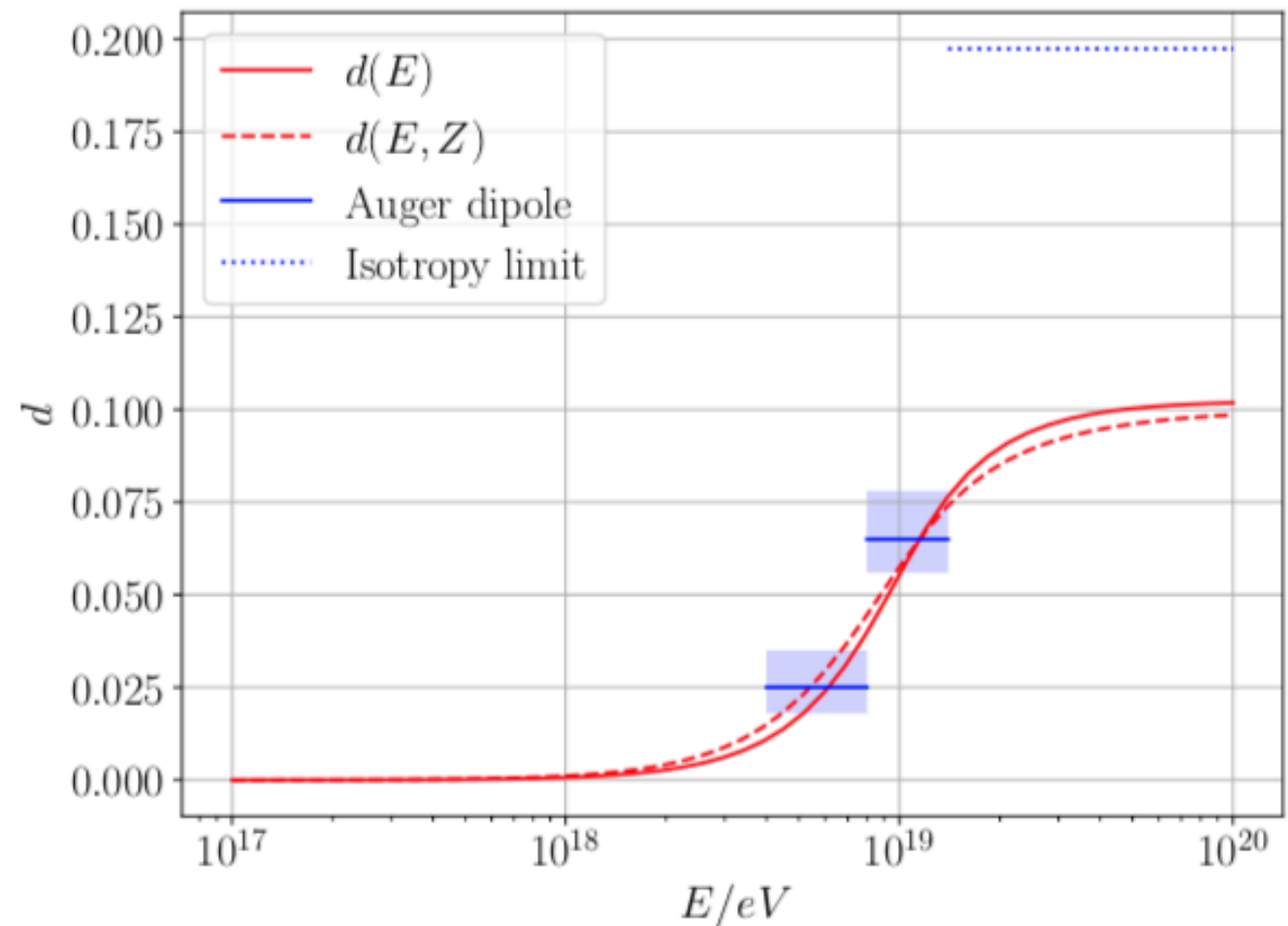
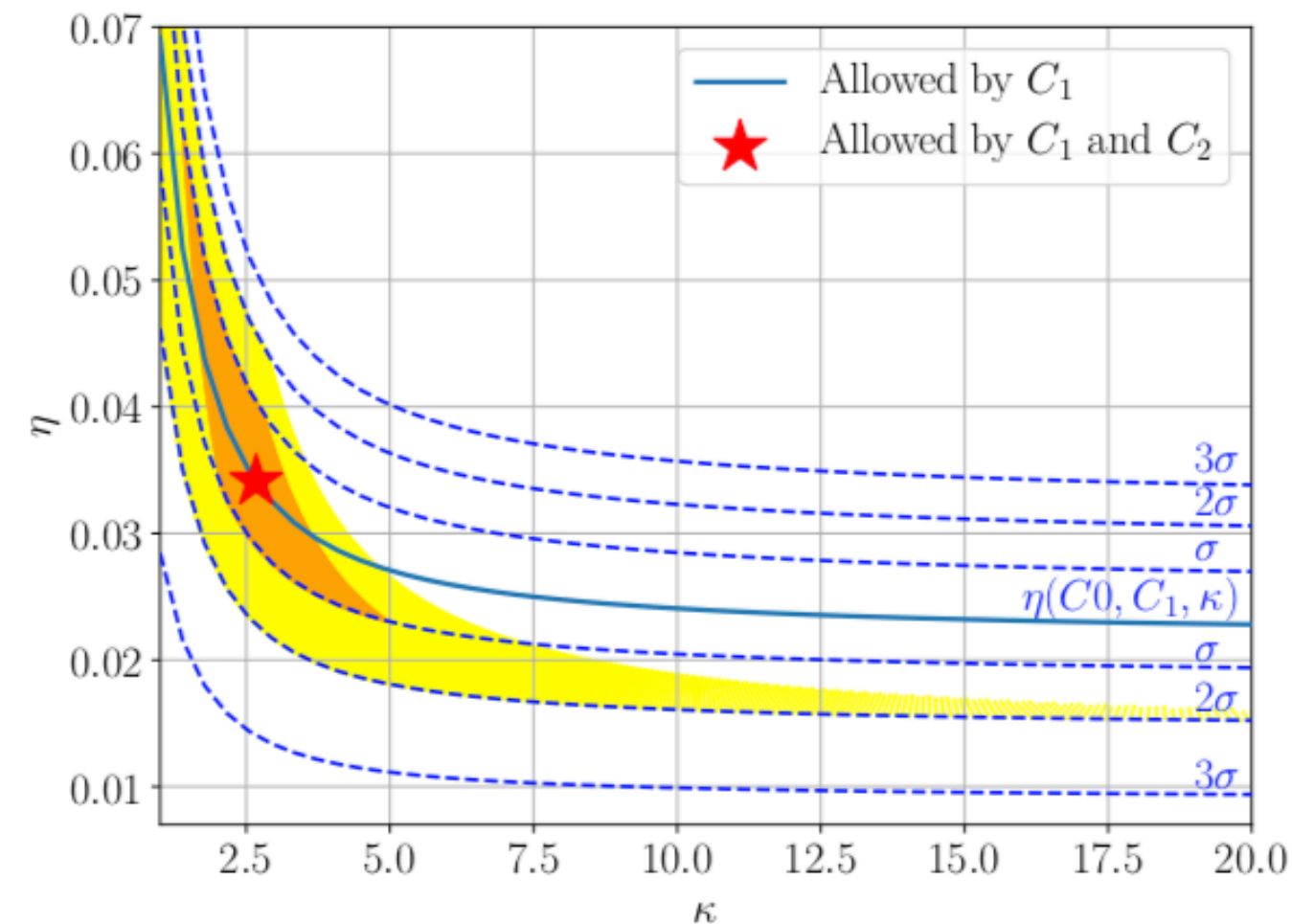
$$\underbrace{\hspace{10em}}_{\gg 1}$$

→ if anisotropies are seen at $E \sim \text{GZK}$, but not at E/Z :

- **there exist protons at GZK producing the anisotropies...**
- **or, if Fe at UHE: $Z \gtrsim 1000 Z_0$... if Si at UHE: $Z \gtrsim 1600 Z_0$... if O at UHE: $Z \gtrsim 100 Z_0$**
 ... sources with such high metallicities?

A Simple One Source + Isotropic Background Model

Contribution of the one discrete source to the total flux parametrised by η and deflection spread by concentration parameter κ : Dipole and quadrupole can fix both parameters, e.g. C_2/C_1 fixes κ



best fit $\eta \sim 0.035$, $\kappa \sim 2.5$, corresponding to a spread of ~ 50 degrees.

Dundovic and Sigl, JCAP 1901 (2019) 018 [arXiv:1710.05517]

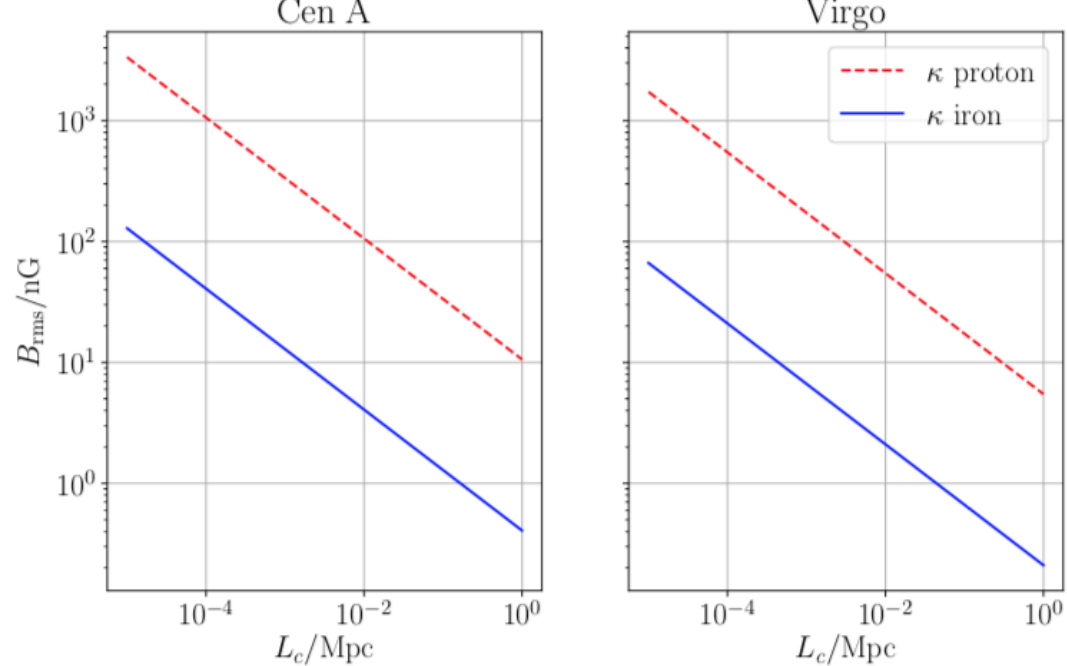


Figure 12. For a source of a given distance, the remaining parameters left undetermined are charge, magnetic field strength and coherence length. The plot shows the relation between B_{rms} and L_c following from eq. 3.4 for the fitted value of κ , for proton and iron primaries coming from Centaurus A and the Virgo cluster.

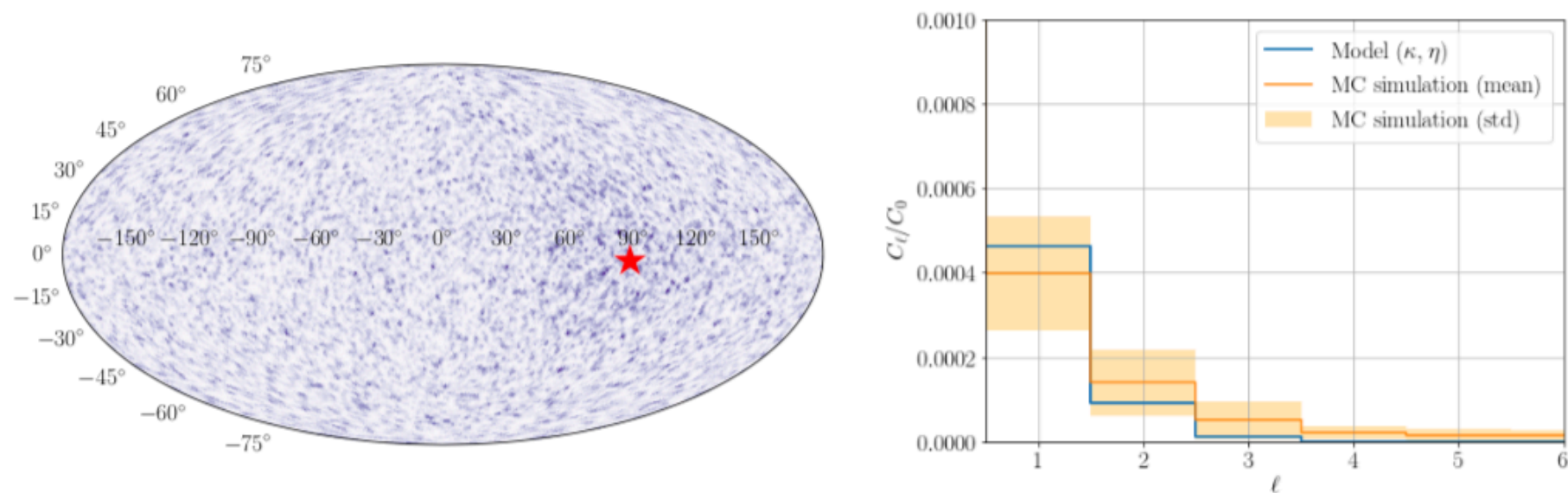


Figure 13. The two plots are results of a Monte Carlo simulation which is set up as described in the text. The sky plot shows the dipole induced by the single source which is placed at 4 Mpc distance from the observer. The direction of the dipole is marked with the star. Other parameters are $Z = 26$, $E = 11.5 E_{\text{TeV}}$, $B_{\text{rms}} = 2.9 \text{ nG}$, $L_c = 30 \text{ kpc}$, $\eta = 0.03$ where $(1 - \eta)$ is the isotropic contribution from the background. The right panel plot depicts the first few moments of the angular power spectrum where the blue line is the analytically calculated spectrum by using the spread parameter (κ) and the relative flux (η), while the orange line is a fit from the simulation. The orange shaded area represents one sigma fluctuations.

Dundovic and Sigl, JCAP 1901 (2019) 018
[arXiv:1710.05517]

Some general Requirements for Sources

Accelerating particles of charge eZ to energy E_{\max} requires induction $\epsilon > E_{\max}/eZ$. With $Z_0 \sim 100\Omega$ the vacuum impedance, this requires dissipation of minimum power of

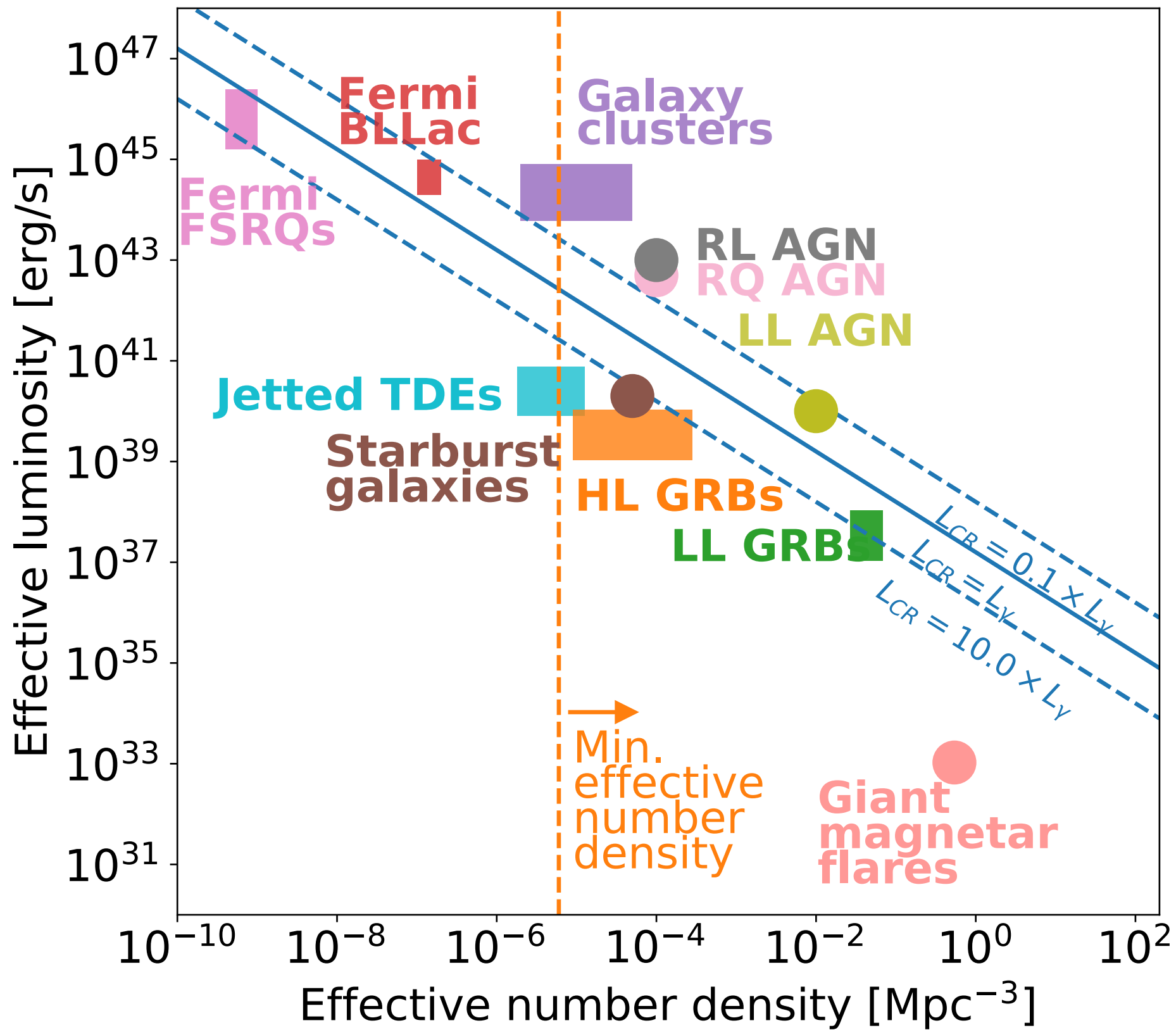
$$L_{\min} \sim \frac{\epsilon^2}{Z_0} \simeq 10^{45} Z^{-2} \left(\frac{E_{\max}}{10^{20} \text{ eV}} \right)^2 \text{ erg s}^{-1}$$

This „Poynting“ luminosity can also be obtained from $L_{\min} \sim (BR)^2$ where BR is given by the „Hillas criterium“:

$$BR > 3 \times 10^{17} \Gamma^{-1} \left(\frac{E_{\max}/Z}{10^{20} \text{ eV}} \right) \text{ Gauss cm}$$

where Γ is a possible beaming factor.

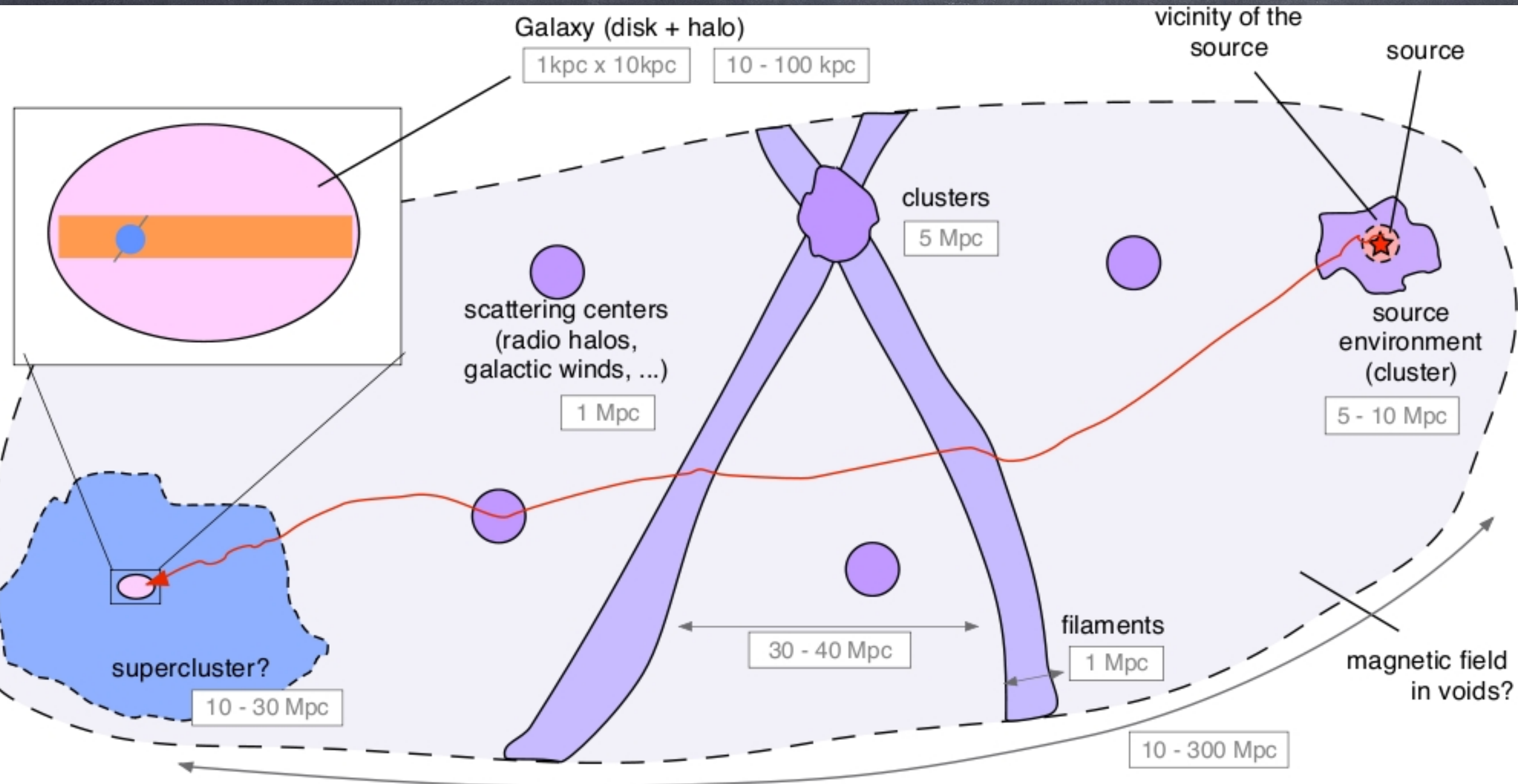
If most of this goes into electromagnetic channel, only AGNs and maybe gamma-ray bursts could be consistent with this.



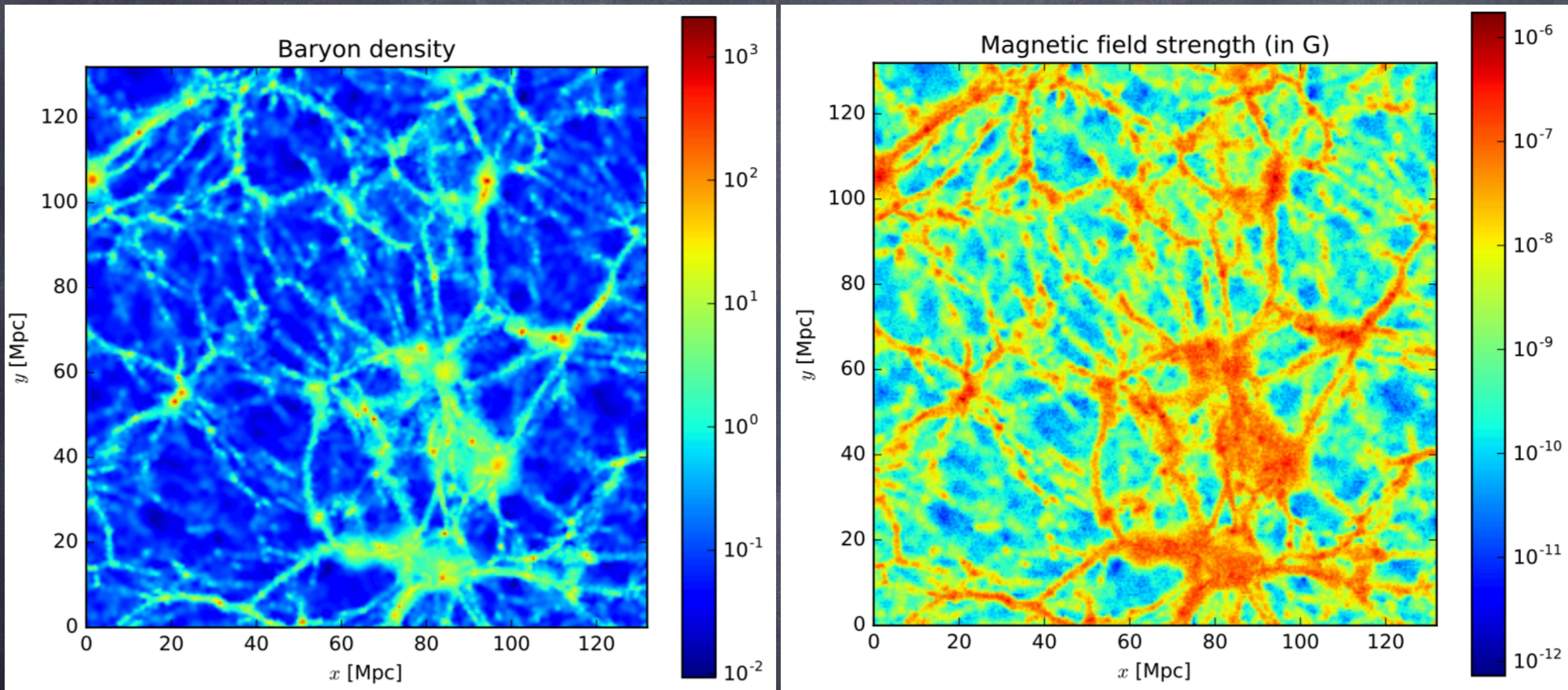
luminosity versus number density for continuous sources or (total energy released)/T versus (rate per volume)*T for intermittent sources with effective time delay $T=3 \times 10^5$ y:

diagonal lines from UHECR flux, minimal number density from lack of significant UHECR clustering

Modelling Cosmic Rays in the Structured Universe

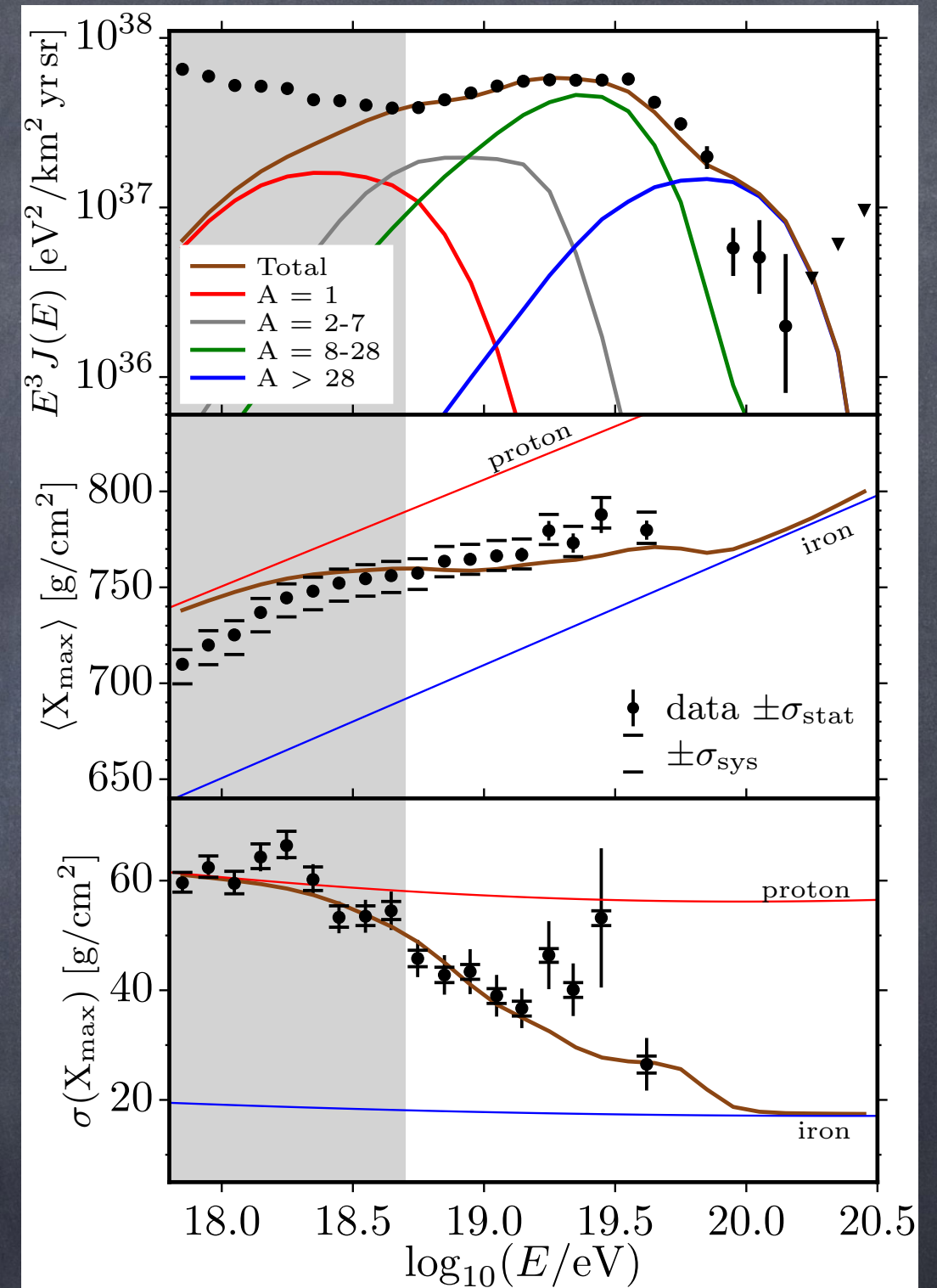
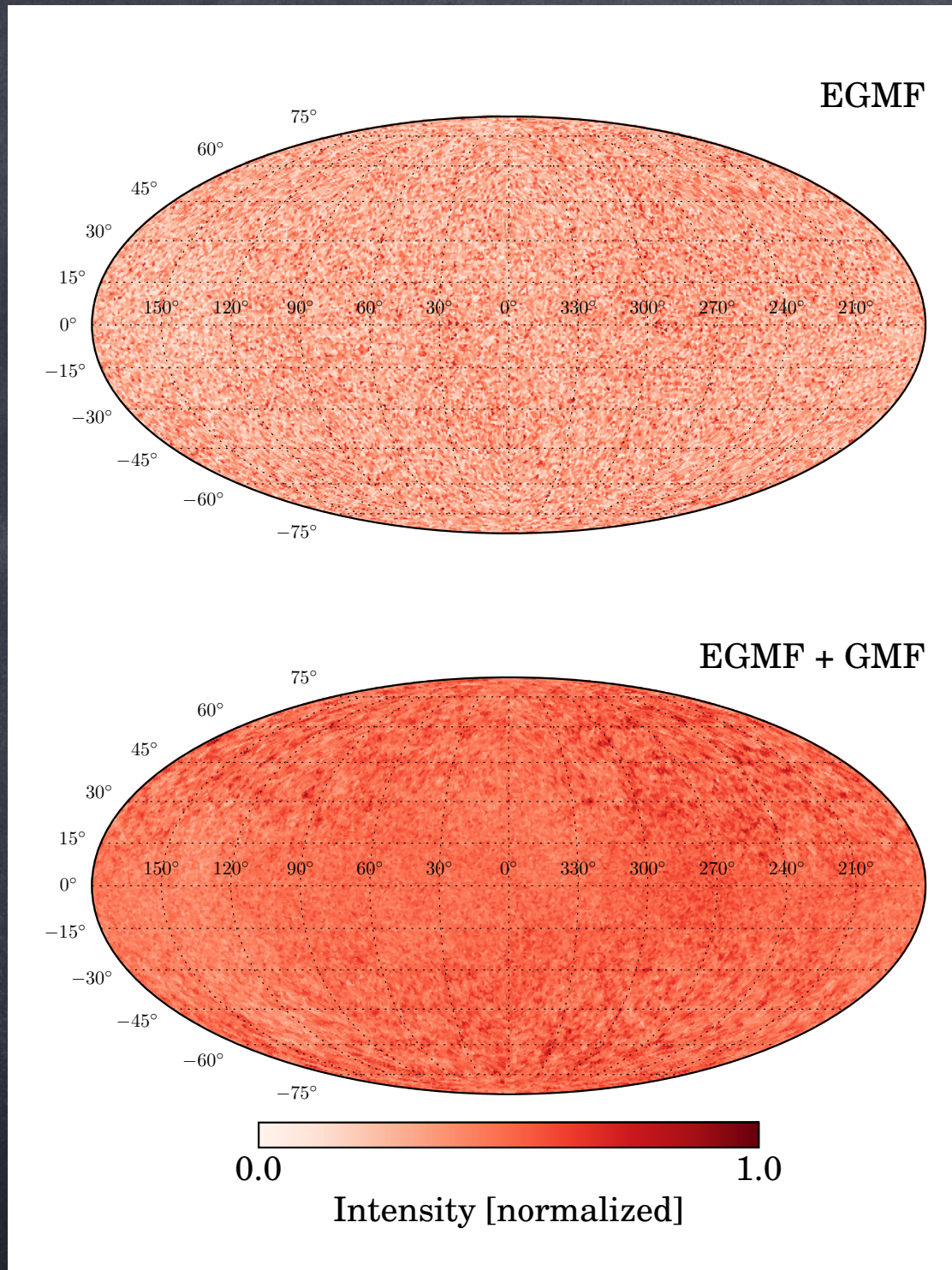


Discrete Sources in nearby large scale structure and structured magnetic field



Challenge: Unconstrained/constrained large scale structure simulations often have too limited spatial extent to cover all relevant sources below the GZK energy. Can be partly cured by period boundary conditions which can, however cause artificial regularities in simulated sky maps for small deflections (as can source distributions centered on Earth)

Building Benchmark Scenarios



combining spectral and composition information with anisotropy can considerably strengthen constraints on source characteristics, distributions and magnetization

G. Sigl, book "Astroparticle Physics: Theory and Phenomenology", Atlantis Press/Springer 2016, based on David Walz, Pierre Auger collaboration

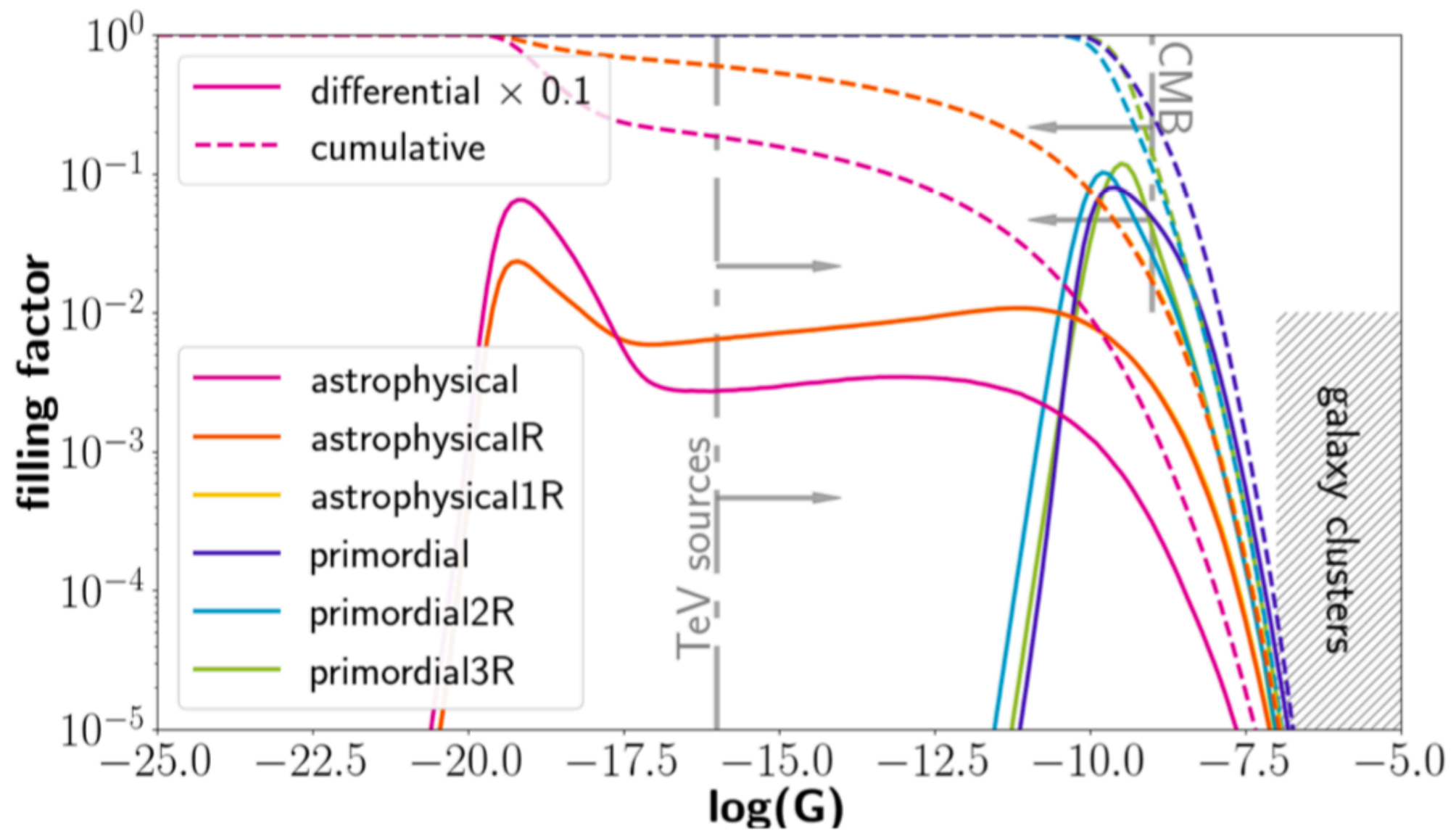


Figure 2. Volume filling factor of the models listed in Tab. 1. The solid lines show the differential filling factor renormalized by 0.1 for clarity, dashed lines show the cumulative filling factor. The grey arrows and shaded area indicate the limits given from observations as listed in the introduction. The yellow line of the *astrophysical1R* model fits exactly with the *astrophysicalR* model.

Simulated Predictions of angular Multipoles

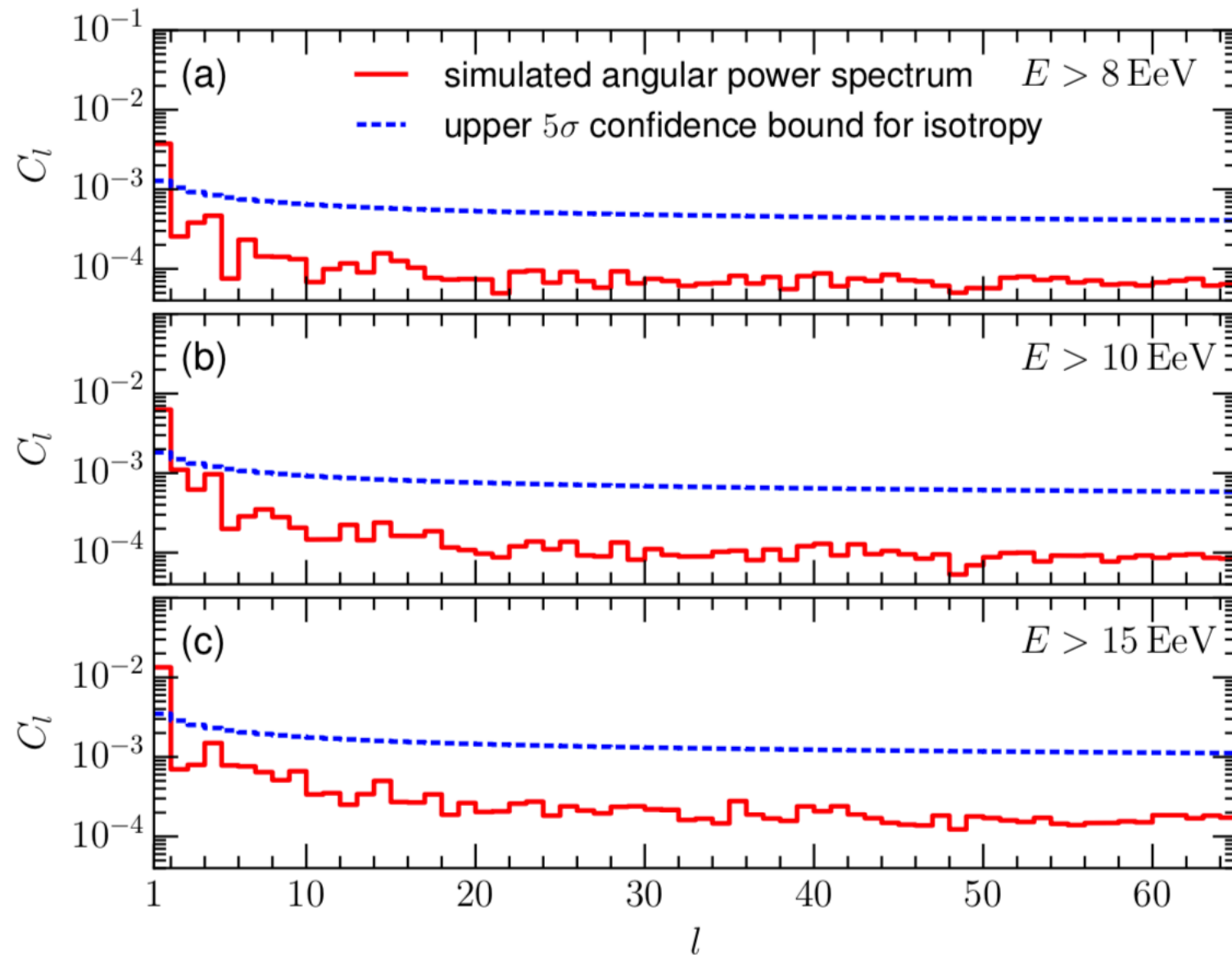


Figure 1. Angular power spectrum (solid red curves) for the arrival directions of the simulated UHECR reaching the observer with energies (a) $E > 8 \text{ EeV}$, (b) $E > 10 \text{ EeV}$, and (c) $E > 15 \text{ EeV}$ as well as the corresponding upper 5σ confidence bounds for isotropy (dashed blue curves). For all energy intervals there is a significant dipolar anisotropy (see the values of $C_1(E)$), whereas the higher-order $C_l(E)$ are compatible with isotropy.

Wittkowski, Kampert, *Astrophys. J.* 854 (2018) L3
[arXiv:1710.05617]

based on the “benchmark model” which combines constrained large scale structure simulation with magnetic field strength distribution of Miniati model

inclusion of EGMF also leads to softer best fit injection indices $\gamma \sim 1.6$ [Wittkowski, proceedings of ICRC 2017]

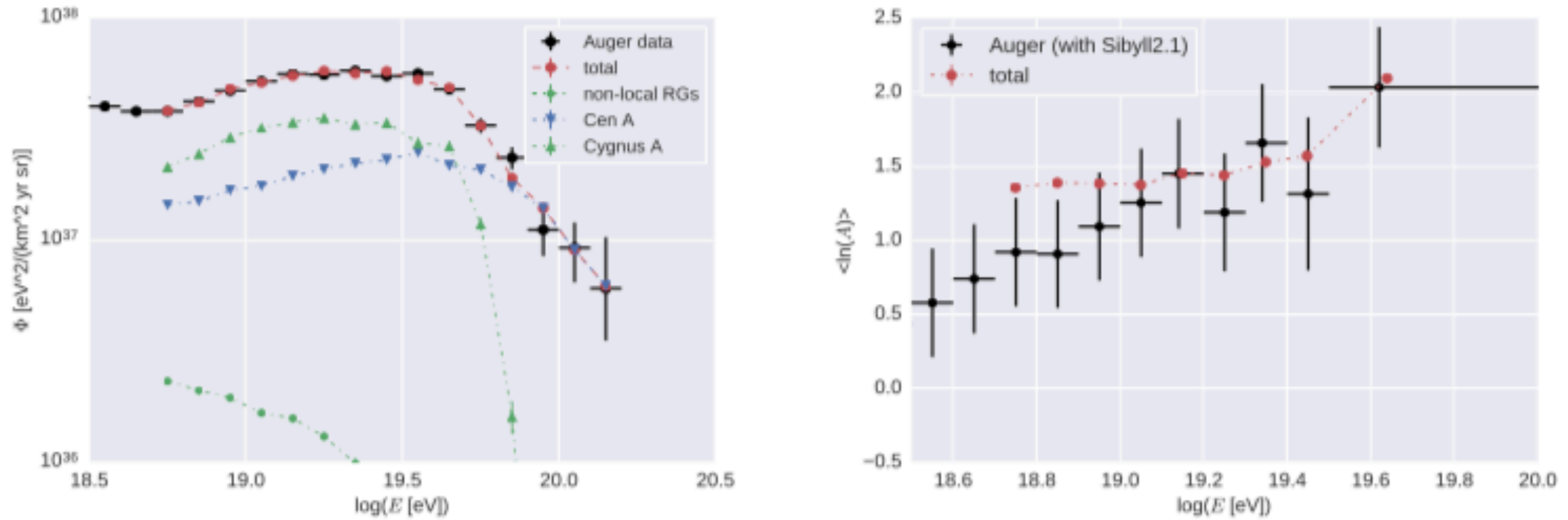


Figure 11. Best-fit results to energy spectrum (left) and chemical composition (right) using Sibyll2.1 and the heavy composition scenario with powerful Centaurus A.

based on a catalogue of radio galaxies where each source has individual injection parameters based on radio luminosity at 1.1 GHz, $Q_{\text{cr}}=4Q_{\text{jet}}/7$, $L_{\star}=4.9 \times 10^{40}$ erg/s:

$$\hat{R} \equiv \frac{E_{\text{max}}}{Z e} = \frac{\beta_{\text{sh}}}{f_{\text{diff}}} B r = g_{\text{acc}} \sqrt{\frac{g_{\text{cr}} Q_{\text{jet},0}}{c}} = \frac{g_{\text{acc}}}{e} \sqrt{\alpha_f \hbar g_{\text{cr}} Q_{\text{jet},0}} .$$

$$Q_{\text{cr}} \simeq 1.3 \times 10^{42} g_{\text{cr}} \left(\frac{L_{1.1}}{L_{\star}} \right)^{6/7} \frac{\text{erg}}{\text{s}} ,$$

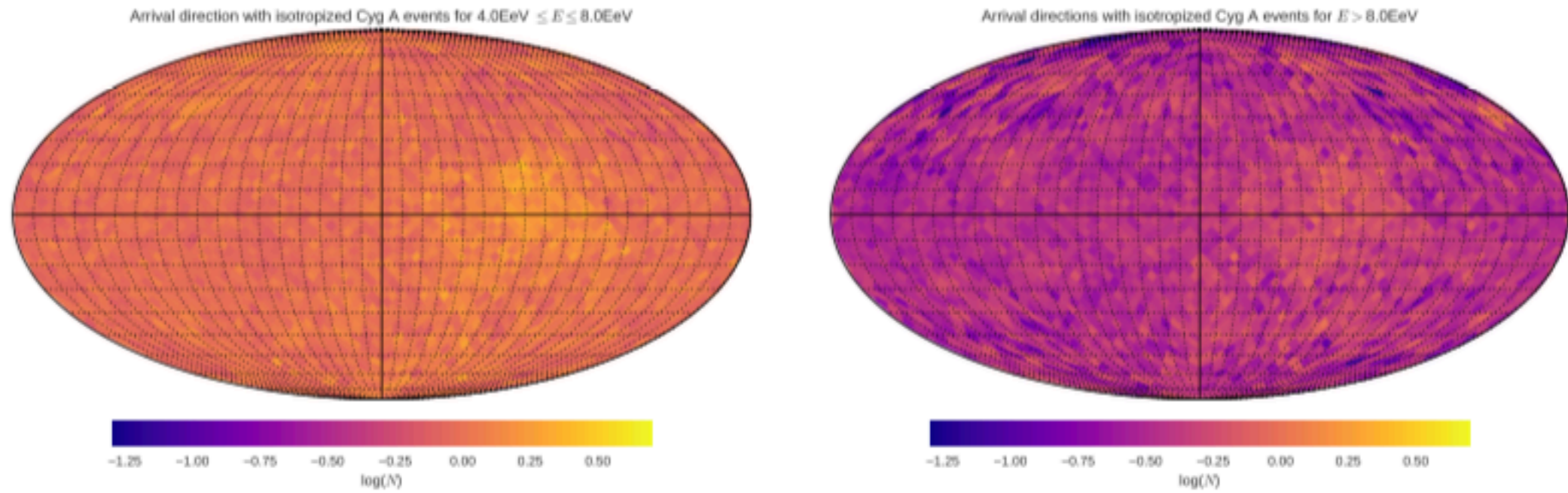


Figure 13. Skymap with isotropized Cygnus A events for $4 \text{ EeV} \leq E \leq 8 \text{ EeV}$ (left), and $E > 8 \text{ EeV}$ (right) using Sibyll2.1 and the light composition scenario with a powerful Centaurus A.

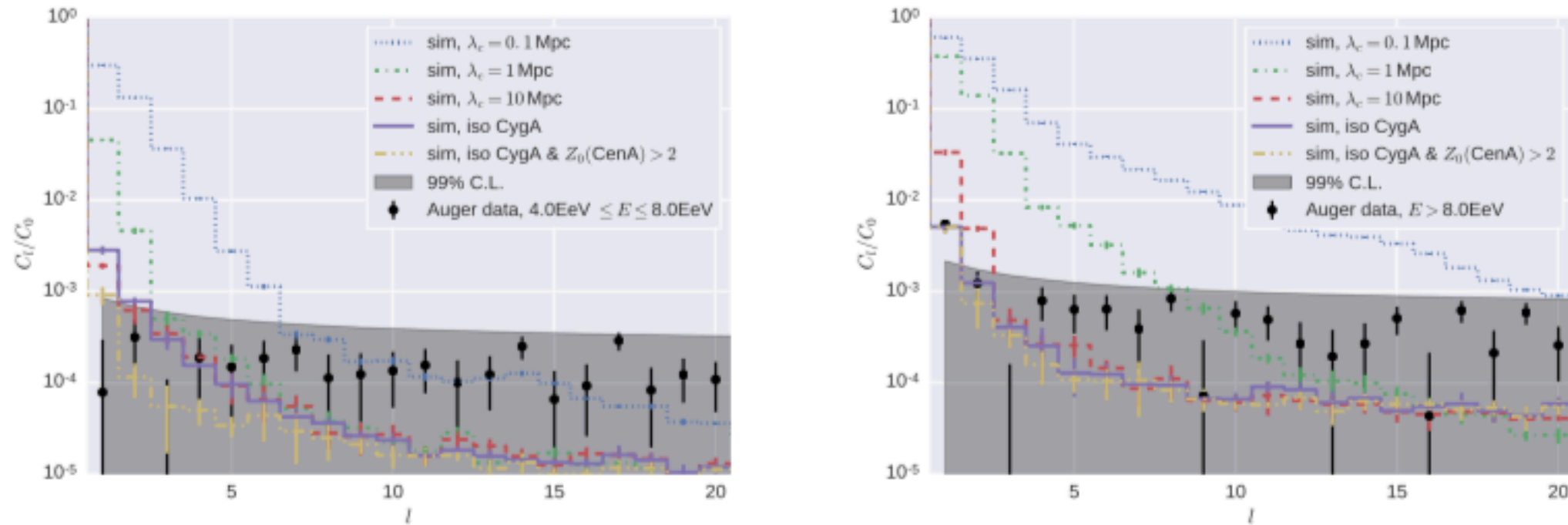


Figure 14. Angular power spectrum with isotropized (solid and dash-dotted line) and non-deflected (dashed line) Cygnus A events for $4 \text{ EeV} \leq E \leq 8 \text{ EeV}$ (left), and $E > 8 \text{ EeV}$ (right) using Sibyll2.1 and the light composition scenario with a powerful Centaurus A.

Conclusions

- 1.) A dipolar anisotropy unrelated to the Galactic plane of amplitude $\sim 6.5\%$ has been observed above 8×10^{18} eV
- 2.) Data indicate a growth of the dipolar amplitude from 4 to 32 EeV and beyond
- 3.) Indications for intermediate scale anisotropies associated with extragalactic gamma-ray sources are found above 4×10^{19} eV
- 4.) Amplitude of anisotropies may be dominated by source distributions/most nearby sources. Magnetic fields may shift directions and mix dipoles; disentangling both influences will be a challenge